

Manuscript Number: JASC18-124R2

Title: Landmark of the Past in the Antequera Megalithic Landscape: A Multi-Disciplinary Approach to the Matacabras Rock Art Shelter

Article Type: Full length article

Keywords: Iberian schematic rock art; Multi-disciplinary study; digital image analysis; U-Th dating; Antequera Megalithic landscape

Corresponding Author: Dr. Leonardo Garcia Sanjuan, PhD

Corresponding Author's Institution: University of Seville

First Author: Miguel Ángel Rogerio-Candelera, PhD

Order of Authors: Miguel Ángel Rogerio-Candelera, PhD; Primitiva Bueno Ramírez, PhD; Rodrigo De Balbín-Behrmann, PhD; M. Isabel Dias, PhD; Leonardo Garcia Sanjuan, PhD; Mathilda L Coutinho, PhD; José Antonio Lozano Rodríguez, MSc; Ana Z Miller, PhD; Alistair W Pike, PhD; Christopher D Standish, PhD; M. Isabel Prudêncio, PhD; A.L. Rodrigues; José María De la Rosa Arranz, PhD; Diego Gaspar

Abstract: The background of this paper is the biographical relationship between the Menga dolmen and La Peña de los Enamorados mountain (a conspicuous and highly-recognisable natural formation), both part of the Antequera megalithic landscape. Our main aim is to provide a high-resolution characterisation of the Matacabras rock art shelter, located on the northern side of La Peña de los Enamorados. This is achieved through a photogrammetric topographic survey, a detailed assessment of the graphic motifs identified through the use of digital image processing and various types of physical and chemical analysis, a geo-chemical characterisation of pottery found on its surface, and a comparative stylistic analysis of its motifs. Our study suggests that Matacabras (and the site of Piedras Blancas I, located just below it), played an important role in the genesis of Menga, which perhaps makes it the most important rock art location of Spanish Late Prehistory.

1 ***Landmark of the Past in the Antequera Megalithic Land-***
2 ***scape: A Multi-Disciplinary Approach to the Matacabras***
3 ***Rock Art Shelter.***

4

5 Miguel Ángel Rogerio-Candelera, Primitiva Bueno Ramírez, Rodrigo de Balbín Behr-
6 mann, M. Isabel Dias, Leonardo García Sanjuán, Mathilda L. Coutinho, José Antonio
7 Lozano Rodríguez, Ana Z. Miller, Alistair W. Pike, Christopher D. Standish, M. Isabel
8 Prudêncio, A.L. Rodrigues, José M. de la Rosa Arranz and Diego Gaspar

9

10

11

12 ***Abstract***

13

14 The background of this paper is the biographical relationship between the Menga dol-
15 men and La Peña de los Enamorados mountain (a conspicuous and highly-recognisable
16 natural formation), both part of the Antequera megalithic landscape. Our main aim is
17 to provide a high-resolution characterisation of the Matacabras rock art shelter, lo-
18 cated on the northern side of La Peña de los Enamorados. This is achieved through a
19 photogrammetric topographic survey, a detailed assessment of the graphic motifs
20 identified through the use of digital image processing and various types of physical and
21 chemical analysis, a geo-chemical characterisation of pottery found on its surface, and
22 a comparative stylistic analysis of its motifs. Our study suggests that Matacabras (and
23 the site of Piedras Blancas I, located just below it), played an important role in the
24 genesis of Menga, which perhaps makes it the most important rock art location of
25 Spanish Late Prehistory.

26

27

28 **1. Introduction: an exceptional landscape**

29
30 On July 15th 2016, the General Assembly of UNESCO, gathered in Istanbul (Turkey),
31 approved the inclusion of the Antequera Dolmens Site (Málaga, Spain) in the World
32 Heritage List. This site comprises three megalithic monuments and two natural forma-
33 tions. The megalithic monuments are Menga and Viera (built during the Late Neolithic
34 period) and the El Romeral tholos (erected during the Copper Age). The natural
35 monuments are El Torcal karstic formation, located some 11km south of the megaliths,
36 and the mountain known as La Peña de los Enamorados ('The Lovers' Rock') located
37 6km east of Menga and Viera and scarcely 2km from El Romeral tholos (Figure1).

38
39 The Outstanding Universal Values (OUVs) recognized in the UNESCO Declaration meet
40 selection criteria 1, 3 and 4 which are reflected in the exceptional architecture, biogra-
41 phy and landscape of the megalithic monuments and their association with the natural
42 formations. Their architectural design and intrinsic properties make these three mega-
43 liths unique. Menga and El Romeral are also the largest stone monuments from the
44 Late Neolithic and Copper Age Iberia and represent exceptional feats of prehistoric
45 engineering (see Lozano Rodríguez et al. 2014 or García Sanjuán and Lozano Rodríguez
46 2016 for more detailed descriptions). Recent studies suggest that these three monu-
47 ments had exceptionally long life-histories spanning Late Prehistory, Iron Age, Antiq-
48 uity, the Middle Age and even Modern History. Menga was repeatedly used as a burial
49 ground between the 4th and 11th centuries AD. Later, it was used as a sheepfold, dwell-
50 ing or perhaps for water supply through the well inside it (García Sanjuán and
51 Wheatley 2010, Diaz-Zorita Bonilla and García Sanjuán 2012, Aranda Jiménez et al.
52 2015, García Sanjuán et al. 2016, García Sanjuán and Lozano Rodríguez 2016, Bradley
53 and García Sanjuán 2017, Bueno Ramírez et al. 2018).

54
55 The background to our study is the relationship between Menga and La Peña de los
56 Enamorados. This relationship has two major conceptual dimensions: landscape and
57 biography. They are expressed through a complex connection between the architec-
58 ture, the mountain, the rock art found in it and the visibility patterns between them.
59 As we will show in this paper, there is strong evidence suggesting that La Peña de los
60 Enamorados played an important role in the genesis of Menga, which perhaps makes
61 the Matababras shelter the most important rock art location of Spanish Late Prehis-
62 tory. Although previous studies have briefly described this shelter, no integral study of
63 the Matababras shelter had been carried out until now. In our study, we will first de-
64 scribe the shelter's topography based on the results of high resolution photogram-
65 metry, before moving onto a detailed assessment of the graphic motifs identified
66 through the use of digital image processing and various types of physical and chemical
67 analysis and then looking into the geochemical composition of the surface pottery
68 found nearby. In the discussion, we will evaluate the chronology and the conceptual,
69 visual and symbolic relationship of Matababras, and the mountain it is part of, with
70 Menga.

71 72 **2. Background**

73 74 **2.1. Location**

75
76 Geologically, La Peña de los Enamorados (henceforth, La Peña) is a prominent eleva-
77 tion in the Baetic cordillera, the westernmost edge of the European Alpine mountain
78 system formed in the Miocene. Within the Antequera landscape, La Peña appears as a
79 huge limestone outcrop with a North-South orientation. It rises to 880 metres above
80 sea level, visually dominating the Antequera plain. Its West, East and northern faces
81 present very steep slopes. There is an imposing sheer cliff nearly 100 meters high on
82 its northern face; the Matababras rock art shelter is located at the foot of this cliff.

83
84 La Peña stands somewhat isolated within the Quaternary depression of the Antequera
85 plain. This massive rock belongs to the External Subbetic of Jurassic age and is flanked
86 at the South by the materials of Triassic age belonging to the Antequera Trias (Sanz de
87 Galdeano et al., 2008), and further South still by the elevations of the El Torcal karst
88 system (Jurassic period) that belongs to the Internal Subbetic (Figure 2A). To the North
89 it is bordered by the Guadalquivir complex (Guarnido Olmedo 1977). These materials
90 are rich in abiotic resources that were used throughout Late Prehistory, including flint
91 (Morgado-Rodríguez et al., 2011), marble (Martínez-Sevilla et al., 2011), ophite (Mor-
92 gado Rodríguez and Lozano Rodríguez, 2011) as well as salt, iron oxides and peridotites
93 (Figure 2A). The wealth of materials in and around this region makes the Antequera
94 Trias unique within the Baetic mountain range, which is probably connected to the
95 high number of archaeological sites.

96
97 The lithostratigraphic scheme of La Peña shows (Figure 2B) a succession of dolomites,
98 oolitic limestone as well as red, nodular limestone formed during the Jurassic and pink
99 marlstone and marl-limestone from the Cretaceous period (García Sanjuán et al. 2015:
100 fig.13). The stratigraphic and sedimentological characteristics of the sediments reveal
101 the typical successions of the Internal Subbetic domain, with a pelagic threshold de-
102 veloped over much of the Middle-Late Jurassic. These Jurassic facies (Ammonitico
103 Rosso) present beige to pink colouring and a large amount of pelagic micro-fauna,
104 mainly ammonites. Being less resistant to erosion, differential progression can be seen
105 in the formation of the northern vertical cliff of La Peña, where the Matababras shelter
106 is located.

107
108 Historically, La Peña has been a well-known landmark within its immediate geographi-
109 cal setting, not only due to its commanding visual presence, but also because of its
110 remarkable anthropomorphic silhouette when seen from the West or East, especially
111 when the sun is low, at dawn or at sunrise (Figure 3A). It is therefore not surprising
112 that this mountain has traditionally served as a landmark for terrestrial navigation
113 along the two major routes that cross at Antequera: the West-East route connecting
114 the lower Guadalquivir valley (Seville) with the Granada and Guadix-Baza basins to-
115 wards eastern Spain (Levant), and the North-South route connecting the Mediterra-
116 nean (Málaga) to the interior of the Guadalquivir valley (Córdoba) towards the Spanish
117 central plateau. The finding of a Roman milestone belonging to the route connecting
118 Antikaria (Antequera) with Iliberris (Granada) on its southern foot, where the Guadal-
119 horse river flows, proves that La Peña was a major place of transit in Antiquity (Gozal-
120 bes Cravioto 1986). With Antequera being a crossroad and major place of transit, La

121 Peña was the landmark announcing its presence from several kilometres away to those
122 travelling from the East, West or North (it is less visible from the South).

123

124 The topographical importance of this mountain is well reflected in the local folklore.
125 The legend that gives the mountain its name very likely originated in the 15th century
126 CE when the Castilian kingdom of Seville and the Nasrid kingdom of Granada fought for
127 control of the region. According to this legend, of which there are various versions, a
128 Muslim man and a Christian woman fell in love, a relationship not accepted by either
129 of their families. After an unsuccessful escape, the lovers decided to take their lives,
130 throwing themselves from the northern cliff of La Peña (Jiménez Aguilera 2006) (Fig-
131 ure3B). It cannot be ruled out that, as so often happens in Iberian folklore, the medie-
132 val legend is rooted in much older “pagan” traditions related to La Peña’s strongly an-
133 thropomorphic silhouette, also portrayed locally as a dormant giant woman (García
134 Sanjuán and Wheatley 2010: 26). In fact, La Peña is a major archaeological complex
135 with evidence of occupation and frequentation throughout the Neolithic, Copper and
136 Bronze Ages (Moreno Aráquez and Ramos Muñoz 1983, Rodríguez Vinceiro et al. 1992,
137 Suárez Padilla et al. 1995), Antiquity (Cisneros Franco and Corrales Aguilar 1994) and
138 the Middle Ages.

139

140 **2.2. Discovery and Previous Studies**

141

142 Before its re-discovery in April 2006 caused its definitive inclusion in the on-going re-
143 search of the Antequera megalithic landscape (García Sanjuán and Wheatley 2009:
144 139-142), the Matababras rock shelter had already been cited in a number of publica-
145 tions, first mentioned as “La Peña shelter” (Muñoz Vivas 1991: 509, Maura Mijares
146 2003, Maura Mijares 2005, Cantalejo Duarte et al. 2010), and later as “Matababras
147 shelter” (Maura Mijares et al. 2007, Maura Mijares 2011, Martínez García 2013, Bueno
148 Ramírez et al. 2009, Bueno Ramírez and De Balbín-Behrmann 2009, De Balbin-
149 Behrmann et al. 2017). All these references are general and included in a wider re-
150 search framework.

151

152 In summary, although several descriptions of Matababras have been published to date,
153 all of them are rather fragmented and brief. The longest of these descriptions, pub-
154 lished in Spanish by Maura Mijares (2011), is only three pages long.

155

156 Therefore, considering the precedents mentioned above, this paper has a threefold
157 aim: (i) to provide the first in-depth multi-disciplinary characterisation of this impor-
158 tant site; (ii) to place it within its spatial and chrono-cultural context which is none
159 other than the Antequera megalithic landscape; (iii) to make this knowledge accessible
160 to an international audience through an English language paper.

161

162 **3. A Multi-Disciplinary Approach**

163

164 **3.1. Topographic Survey**

165

166 The topography and precise shape of the Matababras shelter have been recorded us-
167 ing three-dimensional (3D) photogrammetric modelling supported by geo-positioning

168 techniques. Geo-positioning was carried out using a GPSTrimbleR6 receiver using the
169 RTK (Real Time Kinematic) method, which connects the equipment in real time to the
170 Andalusian Positioning Network (RAP in its Spanish acronym), with a maximum error of
171 1 cm. Reference points inside the shelter were located using a Trimble 5600 DR200+
172 total station as in this area it is not possible to reach the satellite network coverage.
173 Photogrammetric modelling was achieved using Structure from Motion (SFM), which
174 allows three-dimensional models to be obtained from unstructured image data and
175 with un-calibrated cameras (Meyer and Gaspar 2017). This technique enables a 1:1
176 three-dimensional model with digital realistic textures to be obtained, providing all the
177 necessary data on the studied area at any time. For this study the AgisoftPhotoscan,
178 version 1.2.5. build 2614 (Agisoft LLC, St. Petersburg, Russia) software package was
179 used.

180
181 The photogrammetric survey provides a good base for the graphic depiction of the
182 motifs. On the western side of the shelter there are various motifs painted in red
183 which follow a distinctly vertical pattern. This side is significantly affected by black col-
184 our run-offs on the walls(Figure 4), caused both by rain as well as irregular water leaks
185 characteristic of the mountain's karst system. Running all along the floor of the shelter,
186 which is rocky and uneven, the photogrammetric model shows up to three deep, sub-
187 circular cavities which are possibly interconnected and which are currently filled with
188 sediments. These cavities have not been excavated, but visual inspection and the ren-
189 dering of the photogrammetric model suggests that they may be human-made (Figure
190 5) which would reinforce the social and cultural importance of the shelter. Similarly to
191 the case of Matababras, at the shelters of Buraco da Pala and Fraga d'Aia, in northern
192 Portugal, panels of schematic rock art were found in connection with negative features
193 interpreted as a dwelling and storage area (Sanches 2003:167-168).

194

195 **3.2. Digital Image Analysis**

196

197 Following the topographic survey and photogrammetric restitution, a major aim of this
198 study was to produce a new integral drawing of the painted motifs based on different
199 digital imaging techniques. To this end, conventional RGB images taken with a digital
200 Canon EOS 450D camera on a conventional tripod with two bubble levels have been
201 used as primary material. The presence of the black coatings and the difficulty of ap-
202 preciating the paintings (produced with a red pigment) make it advisable to use a
203 blended focus, which proved to be very useful in mapping both the painting and the
204 black coatings (Figure 6). In order to process the raw images we have used Principal
205 Component Analysis (Portillo et al 2008, Rogerio-Candelera and Élez Villar 2010,
206 Rogerio-Candelera et al. 2010, 2011, 2013) and Contrast Stretch in HSI colour mode
207 (HSI-CS) technique, as well as an improvement of this technique that we denominated
208 HSI-ECS elsewhere (Rogerio-Candelera 2015, Rogerio-Candelera and Linares Catela
209 2015). In addition, we have applied algebraic techniques such as the ferric pigments
210 index, (for example Sebastian López et al. 2013), as well as additions and subtractions
211 of bands. For these calculations, we used both HyperCube software (US Army Corps of
212 Engineers, Alexandria, VA, USA), specifically targeting this work, with multi- and spec-
213 tral images and ImageJ software (National Institutes of Health, Bethesda, MA, USA),

214 originally designed for biomedical applications but which has been applied to many
215 other scientific disciplines, including rock art recording.

216

217 **3.3. Colour Measurement**

218

219 The colorimetric coordinates of various painted motifs and the rock support (Figure 7)
220 were determined in the CIELAB colour space
221 (<http://www.cie.co.at/index.php/Publications/Standards>). This was made for two rea-
222 sons: firstly, to present the colour of the different painted motifs in a reproducible
223 fashion; and secondly, to obtain an initial classification of the pigments which would
224 allow us to draw up a hypothesis on the existence of more than one phase in the
225 elaboration of the panel, while also determining the basic components of the pigment
226 according to the registered colour (Elias et al. 2006).

227

228 Colour measurements were performed using a portable spectrophotometer (Mi-
229 croflash, Datacolor International). The optical system of the measuring head uses dif-
230 fuse illumination from a pulsed Xenon arc lamp with 0° viewing angle geometry. Col-
231 our coordinates were obtained in the following conditions: D65 illuminant, 10° ob-
232 server and specular component excluded (SCE). The measuring area has diameter of 8
233 mm. Calibration was performed with a white bright tile and a total black light trap.
234 CIELAB method allows characterizing the surface colour by three parameters: L* (light-
235 ness/darkness, varying from white, L* = 100 to black, L* = 0), a* (+a* indicating red and
236 -a* green) and b*(+b* indicating yellow and -b* blue), defined by CIE (Commission
237 Internationale de l'Éclairage). Three colour measurements were performed on each
238 selected sampling-spot, two areas of rock support (Stone 1 and Stone 2) and on the
239 painted areas.

240

241 **3.4. U-Th dating**

242

243 A major aim of this research was to establish the numerical age of the Matababras rock
244 art shelter in order to assess its temporal relationship with the building of Menga. To
245 this end, two carbonate deposits (MC1 and MC2) directly overlying red pigment were
246 sampled for U-Th dating. Detailed sampling methodologies are provided in Pike et al.
247 (2012) and Hoffmann et al. (2016), but briefly: sample locations were mechanically
248 cleaned to remove any surface contamination or alteration, then calcite was collected
249 directly into pre-cleaned plastic sample tubes by scraping with a scalpel. Chemical
250 preparation and isotopic analysis by Multi-Collector Inductively Coupled Plasma Mass
251 Spectrometer (MC-ICP-MS; Thermo Scientific Neptune Plus) was performed at the
252 Ocean and Earth Science analytical geochemistry facilities at the University of South-
253 ampton. Methodologies broadly follow those in Hoffmann et al. (2007), except ion
254 exchange chromatography for the separation of U and Th from the sample matrix em-
255 ployed 0.6 ml columns of UTEVA Spec (Eichrom) resin (Horwitz et al. 1992). Procedural
256 chemistry blank values were always less than 0.01 ng ²³⁸U, 0.1 pg ²³⁵U, 0.01 pg ²³⁴U, 0.01
257 ng ²³²Th and 1 fg ²³⁰Th, respectively.

258

259 **3.5. Field Emission Scanning Electron Microscopy (FESEM) and Pyrolysis-Gas Chroma- 260 tography-Mass Spectroscopy (Py-GC-MS).**

261

262 Three samples of coatings similar to the black ones covering the paintings (labelled
263 MT1 to MT3) were taken by scraping them with a sterile scalpel and stored in Eppen-
264 dorf tubes for electron microscopy as well Py-GC-MS characterisation (Figure 8). The
265 morphology and elemental composition of the black coating samples were studied
266 using field emission scanning electron microscopy (FESEM) combined with energy dis-
267 persive X-ray spectroscopy (EDS). Air-dried samples were directly mounted on sample
268 stubs, sputter coated with gold, and subsequently examined in a FEI's Teneo FESEM
269 (FEI Company, Eindhoven, The Netherlands) equipped with an EDAX (NJ, USA) EDS de-
270 tector using standard ZAF corrections that allow semi-quantitative microanalysis. FE-
271 SEM examinations were operated in secondary electron (SE) detection mode with an
272 acceleration potential of 5kV and 15kV for EDS analyses.

273

274 Py-GC-MS, also known as analytical pyrolysis, was performed using a double-shot pyro-
275 lyser (Frontier Laboratories, model 2020i) attached to a GC/MS Agilent 6890N system.
276 Material from the patina taken at the sample MT2 was carefully grounded; 2 milli-
277 grams were placed in a small crucible capsule and introduced into a preheated micro-
278 furnace at (500°C) for 1 min. The volatile pyrolysates were then directly injected into
279 the GC/MS for analysis. The gas chromatograph column, oven temperature program
280 and mass spectra acquisition were settled according with the conditions reported by
281 Pereira de Oliveira et al. (2011). Compounds were identified using the NIST 05 and
282 Wiley digital libraries and available literature. The relative proportions of the com-
283 pounds satisfactory identified were calculated as the percentage of the total quantified
284 peak area (TQPA), using the main fragment ions (m/z) of each product. Only com-
285 pounds with relative abundances greater than 0.25% were considered. This is a semi-
286 quantitative exercise that allows more detailed description of the results than visual
287 inspection of chromatogram alone.

288

289 **3.6. Neutron Activation Analysis (NAA) and X-Ray Diffraction (XRD) of associated sur-** 290 **face finds.**

291

292 In order to examine the connection between the Matacabras rock shelter and the Late
293 Neolithic activity area of Piedras Blancas I, which lies barely 100 m below, hand-thrown
294 pottery fragments found of the surface of both sites were examined. Two ceramic
295 sherds from Matacabras and five from Piedras Blancas I were analysed for composi-
296 tional characterisation under the assumption that a very similar composition would
297 suggest coetaneous activity. Ceramic pastes were sampled following well-established
298 laboratory protocols (Dias et al. 2010, Prudêncio et al. 2009). Ceramic powder and
299 standards (GSD 9 and soil GSS 1) were irradiated together at the Portuguese Research
300 Reactor, Sacavém. Chemical composition was obtained by instrumental neutron acti-
301 vation analysis (INAA) as described elsewhere (Dias et al. 2013). The following ele-
302 ments were obtained: Na, K, Fe, Sc, Cr, Co, Zn, Ga, As, Br, Rb, Zr, Sb, Cs, Ba, La, Ce, Nd,
303 Sm, Eu, Tb, Yb, Lu, Hf, Ta, Th and U. By using chemical contents as variables, geochemi-
304 cal ratios and normalizations were performed, together with multivariate statistical
305 analyses by means of the Statistica software package (TIBCO Software Inc. 2017), even
306 aware of their restrictions due to the limited amount of cases. Some elements were
307 not considered for the analyses due to their behaviour upon firing (Trindade et al.
308 2011). Mineralogical composition was obtained by X-ray diffraction (XRD) for the bulk

309 material, using a Phillips Pro-Analytical spectrometer with K α Cu source. Non-oriented
310 aggregate powders were prepared and scanned at 1° 2 θ /min from 2° to 70° 2 θ . To es-
311 timate quantities, we measured the diagnostic reflection areas, considering the full
312 width at half maximum (FWHM) of the main minerals (Sanjurjo Sánchez et al. 2010,
313 Trindade et al. 2013) and then weighted by empirical factors or calculated parameters
314 (Biscaye 1965).

315

316

317 **4. Results**

318

319 **4.1. Digital Image Analysis (DIA)**

320

321 The Matacabras graphic motifs were probably produced by applying the paint using
322 the tips of the fingers, resulting in lineal motifs approximately 1 cm wide. The colour of
323 the paint is red, for which reason today they do not stand out greatly against the natu-
324 ral reddish colour of the base rock. Consequently, the different original images used to
325 elaborate the drawings present a high degree of correlation among the three bands.
326 Table1 shows the correlation coefficient matrix of a significant image in the group of
327 images, with correlations between the bands higher than 95%. Thus, the information
328 percentage (variance) is very low for the band of the third principal component, with
329 an average of 0.09% (SD=0.03; $n=10$), indicating that this band is the best to represent
330 the painting. Incidentally, this is the element less represented in the images. Graphi-
331 cally speaking, Figure 6B is a good example of this.

332

333 Although the third principal component is clearly the most suitable in the majority of
334 the images for mapping the painting, possible “false positives” have been controlled
335 using the technique of increasing the contrast, HSI-CS (Gillespie et al. 1986). This tech-
336 nique, developed in the early 1980s to improve the definition of the different image
337 datasets, encompassing the wavelength range to Radar bands (Daily 1983), allows the
338 improvement of the image by intensifying the original colours. Also, the variation of
339 this technique which we have named HSI-ECS (Rogerio-Candelera and Linares Catela
340 2015) produces a colour contrast that allows us to appreciate details more easily and
341 evaluate whether the elements detected using Principal Component Analysis are reli-
342 able or if, on the contrary, they are mere artefacts (Figure 6C). All this has allowed us
343 to elaborate a new tracing of the different elements in the panel (Figure 9).

344

345 **4.2. Colorimetry**

346

347 The colorimetric characterization of the Matacabras paintings was used as a comple-
348 ment to the image analysis to test if the colour measurements could enhance the per-
349 ception of the drawing. Colorimetry itself reveals congruent a^* parameter values with
350 the use of iron oxide-based pigments. Likewise, it detects statistically significant differ-
351 ences between the colour of the supporting rock and the pigments. This allows us to
352 evaluate whether some lines undetected prior to this study are really intentionally
353 painted or are artefacts produced by the documentation methods applied.

354

355 The colorimetric results showed that the a^* value was the main distinguishing feature
356 of the rock paintings, providing the highest chromatic distance between the chromatic
357 coordinates of the natural rock and the painted motifs, the paint values being statisti-
358 cally different from the underlining rock support (Table 2). The only exception was the
359 paint of the great pectiniform motif (Figure 7, sampling points 15 to 17), where the
360 distinction from the rocky substrate was not statistically different - the variability due
361 to the particulate accumulation and the difficulties experienced during the measure-
362 ment acquisition due to the surface irregularities might explain this result. The analysis
363 of the a^* results also showed significant differences between the serpentine 1, an-
364 thropomorph A and the two pectiniforms representations. The enhancement of the
365 coordinate a^* ($+a^*$ indicating red and $-a^*$ green) was expected since natural iron oxide
366 pigments (often termed 'ochres'), were usually the employed pigment in rock art with
367 colour shades between of red and yellow (Gomes et al. 2015). The mineralogical char-
368 acterization of Western Iberian schematic rock art with similar red shades to those of
369 Matacabras showed that pigments could have different minerals such as goethite or
370 hematite (Gomes et al. 2015). Regarding the b^* values no significant differences ($p>0.05$)
371 could be detected between the paint and Stone 1. However, Stone 2 was significant different
372 from all pictograms except anthropomorph A.

373 374 **4.3. U-Th dating**

375
376 Of the two samples collected for U-Th dating, sample MC1 was not processed because
377 its mass was too low for a successful analysis (0.1 mg). Sample MC2 (Figure 10) con-
378 sisted of three sequential sub-samples (MC2a–c), all of which were large enough for
379 analysis (Table 3). However all are characterised by very low ($^{230}\text{Th}/^{232}\text{Th}$), an indicator
380 that detrital thorium, i.e. Th that did not result from in situ decay of uranium, has been
381 incorporated into the calcite – see Pike et al. (2012) and Hoffmann et al. (2016) for
382 further information regarding this issue. High levels of detrital Th contamination typi-
383 cally result in a calculated U-Th age being an overestimation of its true age, and a de-
384 trital thorium correction is required. Here we follow typical procedures and use an
385 assumed detrital ($^{232}\text{Th}/^{238}\text{U}$) of 1.250 ± 0.625 , a value typical of upper crustal silicates
386 (Wedepohl 1995), whilst assuming ^{230}Th and U isotopes are in equilibrium. After apply-
387 ing this correction, the three MC2 sub-samples provide a stratigraphically consistent
388 series of dates from 5.38 ka to 15.85 ka. This correction also reduces the precision of
389 the dates, and after taking this into account the oldest sample indicates that the Mata-
390 cabras art dates to before 5.82 ka BP (c 3800 cal BCE). However, with very high levels
391 of detrital contamination, the corrected date is very dependent on the assumptions
392 used for correction, and we would not normally consider corrected dates with levels of
393 detritus similar to sample MC2 as reliable.

394 395 **4.4. FESEM-EDS examinations**

396
397 The FESEM-EDS examinations of the black patinas collected from the vertical surface of
398 Matababras shelter showed that the bedrock is covered by a discontinuous layer of
399 gypsum crystals (Figure 11A-D). Figure 11B clearly shows that gypsum is the predomi-
400 nant mineral phase, probably due to sulphation processes. Algal-like cells ($< 3 \mu\text{m}$) are
401 discernible on the surface of large gypsum crystals (Figure 11B). Moreover, Na, Cl and K

402 were detected in the black patina, corresponding to salts, mainly halite, which seems
403 to crystallise here (Figure11D). A biofilm composed of algal cells and their metabolic
404 products, particularly extracellular polymeric substances (EPS), are observed in Figure
405 11E. Diatom cells were scarcely observed in the black patina samples (Figure11F).

406

407 The FESEM-EDS data pointed out that the dark-coloured patina at Matababras is asso-
408 ciated with the formation of black crusts of secondary minerals, particularly gypsum,
409 and microbial colonisation. Dark crusts are widespread on stone building surfaces
410 mainly in urban environments (Hermosin et al. 2004, De la Rosa et al. 2017). The in-
411 crease of atmospheric contamination in these environments accelerates stone deterio-
412 ration, especially on limestone where loss is primarily related to dissolution of calcium
413 carbonate induced by the solvent action of acid rainwater. Its penetration into the
414 pores hastens the rate of stone deterioration tremendously, first because water is it-
415 self an effective deteriorating agent, dissolving, hydrating and hydrolysing minerals,
416 and, secondly because it holds in solution substances (carbonaceous particles, sulphur
417 compounds, soluble salts) responsible for leaching of surfaces, pH reduction, dark
418 crusts and efflorescence (Ordóñez et al. 1997, Papida et al. 2000). Gypsum and salt
419 crystallisation evidence weathering mechanisms on the limestone surface of Mata-
420 cabras, suggesting that it has been exposed to atmospheric pollutants, such as sulphur-
421 based compounds. Sulphation has been recognised as one of the main causes of stone
422 deterioration in urban areas (Montana et al. 2008, Rivas et al. 2014). The process starts
423 with the formation of gypsum crusts due to the reaction between sulphuric acid from
424 polluted air and carbonate minerals. Although Matababras is located in a rural envi-
425 ronment, it is near an old railroad for carbon and diesel locomotives which have
426 probably increased sulphur-based compounds in the atmosphere. In addition to sul-
427 phation, phototrophic microorganisms were also observed in the gypsum-rich patina.
428 Their metabolic activity accelerates the dissolution of the carbonate rock due to the
429 release of organic acids which can etch or solubilise stone minerals. Moreover, the
430 slimy surface of biofilms favours the adherence of airborne particles (salts and air pol-
431 lutants) and the accumulation of the moisture on the external layer of the stone (Fer-
432 nandes 2006, Gorbushina 2007).

433

434 **4.5. Pyrolysis-Gas Chromatography Mass-spectrometry (Py-GC-MS)**

435

436 The total ion current (TIC) trace and the list of identified compounds with the percent-
437 ages of TQPA obtained by Py-GC-MS analysis generated at 500°C are reported in Figure
438 12 and Table 4 respectively. The pyrolysates of the Matababras black patina reveal a
439 noteworthy presence of organic compounds, which can be broadly grouped into the
440 following categories: carbohydrates (Ch), aromatic hydrocarbons and derivatives (Ar),
441 N-containing compounds (N-comp), lipids (Lip) and Sulphur containing compounds (S).

442

443 The pyrochromatogram is dominated by Ch which accounted for 13 different com-
444 pounds and over 32.8% of TQPA. The most abundant Ch compounds are furfural, fu-
445 ranes and alpha-*D*-glucopyranose (see peaks 5, 8, 10, 12, 27, 28 or 33; Table 4). Most of
446 theseCh were previously reported as common products of metabolic activities of bac-
447 teria, algae and fungi on rock substrates (Robert and Berthelin 1986), in pyrolysis of
448 endolithic cyanobacteria (Saiz-Jimenez et al. 1990), lichen thalli (Saiz-Jimenez et al.

449 1991), fungal melanins (Saiz-Jimenez et al. 1995) and fungi. The presence of levoglucosan (peak 43) has been previously used as marker of biomass burning (De la Rosa et al. 450 2008). 451

452

453 Aromatic hydrocarbons (Ar) resulted approximately in 20% of TQPA, being dominated 454 by styrene, phenol, toluene, cresols and coumarin derivatives. Anthropogenic pollution 455 sources have been identified as the source of styrene, toluene and numerous light al- 456 kyl aromatic compounds, which may derive from pyrolysis or flash vaporisation of bi- 457 tuminous coal. Acetylcoumarin (peak 44) is found naturally in numerous grasses. Di- 458 methyl-naphthalene and 9, 10-Anthracenedione, 1-amino-4-hydroxy- (peaks 37 and 59 459 respectively) are polycyclic aromatic hydrocarbons typically associated with incom- 460 plete burning of fuel biomass (Schiavon et al. 1995, Standley and Simoneit 1987). Nev- 461 ertheless, benzenes, phenols and methyl phenols are potential pyrolysis products of 462 many biopolymers including amino acids (Moldoveanu 2010), lignin (De la Rosa et al. 463 2012), and proteins.

464

465 The N-containing compounds (N-comp) summed over 21.3% of TQPA. The highest N- 466 comp peaks correspond to pyridine, methyl pyridines and indoles, which are typical 467 pyrolysis products from amino acids and peptides (Moldoveanu 2010). These com- 468 pounds have a biological origin, and are typically synthesised by living organisms (Saiz 469 Jimenez et al. 1995).

470

471 Lipids (Lip) are constituted by a series of *n*-alkanes and *n*-alkenes and several *n*-alkyl 472 fatty acids. They could derive from microorganisms such as cyanobacteria and fungi, 473 plant tissues or soil organic matter. Neophytadiene (peak 49) is a thermal degradation 474 product of chlorophylls (Saiz-Jimenez et al. 1990). It is very abundant in vegetal resins, 475 in addition it could indicate the contribution of algae, which is in fair agreement with 476 the relatively important presence of heptadecane (peak 46), a predominant constitu- 477 ent of most cyanobacteria and algae (Pereira de Oliveira et al. 2011).

478

479 It is also worth noting the presence of sulphur-containing compounds (S). Thiophenes, 480 thiazoles and their derivatives occur in petroleum and coal (Schiavon et al. 1995).

481

482 **4.6. Neutron Activation Analysis (NAA) and X-Ray Diffraction (XRD) of associated sur-** 483 **face finds.**

484

485 The archaeometric characterisation of ceramic artefacts by means of geochemistry and 486 mineralogy is a well established approach to solve technological and provenance issues 487 in pre-historical contexts (Dias et al. 2017). The XRD results enable to define the min- 488 eralogical associations observed for each ceramic fragment (Table 5). Two ceramic 489 samples from Matababras (CerMC2 and CerMC3) and two from Piedras Blancas I (Cer- 490 PBI 2-2 and CerPBI 2-4) are differentiated from the other ones due to the presence of 491 calcite (7%<Calcite<21%) associated to higher amounts of quartz, phyllosilicates, alkali 492 feldspars, plagioclase, and traces of anatase (Figure 12). Only in CerMC3 and CerPBI 2-4 493 samples hematite was detected in traces amounts. Two ceramic sherds (CerPBI 2-1 494 and CerPBI 2-3) have the higher amount of phyllosilicates (>55%), associated to quartz, 495 and traces of alkali feldspars and anatase. The CerPBI 1-1 sample has a different min-

496 eralogical association, with similar proportions of phyllosilicates and quartz (~45%
497 each) and traces of plagioclase, hematite and amphibole. No high temperature phases
498 potentially derived from the calcite or clay minerals (Trindade et al. 2009, 2010) were
499 found in any of the ceramics.

500

501 Seven ceramic samples were chemically analysed by INAA (Table 6) in an attempt to
502 establish chemical correlation between the artefacts found at both sites, with the es-
503 tablishment of groups with similar chemical composition, hence allowing the identifi-
504 cation of the clay materials (Figure 14A). From a chemical point of view one sample
505 CerPBI 1-1 is completely different from all the others, pointing to the use of more ma-
506 fic raw materials, as already indicated by the mineralogical results (amphibole), with
507 lower contents of K, Rb, Cs, LREE, Hf and Ta, and higher contents of Fe, Sc, Cr, Co, Zn,
508 As, Sb and Ba (Figure 14B). Two samples from Piedras Blancas I have similar chemical
509 composition (CerPBI 2-1 and 2-3) with higher amounts of Zr, Ga, REE, Ta, Th. The other
510 four sherds analysed comprise samples from both sites (CerPBI 2-2, 2-4, CerMC 3 and
511 2) with similar chemical composition. Nevertheless sample CerMC2 has higher Cr and
512 Co and lower Zn and Zr contents. It is important to emphasise that these four samples
513 (CerPBI 2-2; 2-4; Cer MC3; 2) are the only ones pointing to the use of calcite-rich raw
514 materials. However, the effect of post-burial chemical alteration must be ruled out as a
515 valid explanation for this observed chemical patterning, and even more detailed stud-
516 ies would help, particularly by scanning electron microscopy. It is important to take
517 into consideration that they all came from the same environment, and only those four
518 are calcite rich. Thus, we may assume the use of different raw materials, and the most
519 relevant, is that these preliminary analytical results yield groups of ceramic sherds with
520 similar composition at both sites, indicating in some cases similar sources for the raw
521 materials.

522

523 **5. Discussion**

524

525 The importance of the Matababras rock art shelter lies not only in its intrinsic charac-
526 teristics, but rather in its close relationship with Menga within the wider framework of
527 the key role that La Peña seems to have played in the genesis and design of this great
528 megalith. The almost exact orientation of Menga's axis of symmetry towards the
529 Matababras shelter (Figure 15) has been interpreted as the commemoration of a place
530 that had special symbolic significance before the dolmen was built (García Sanjuán and
531 Wheatley 2009, 2010, García Sanjuán and Lozano Rodríguez 2016, De Balbín-
532 Behrmann et al. 2017), although astronomy has also been claimed to play a part in the
533 monument's orientation (Lozano Rodríguez et al., 2014).

534

535 Therefore, an obvious key issue in this respect is determining Matababras' chronology.
536 Two immediate problems need to be confronted: firstly, to determine when the paint-
537 ings were made and the shelter used; and secondly, to find out if distinct phases can
538 be differentiated in the usage of the rock shelter.

539

540 In terms of the first issue, radiocarbon dating was ruled out due to the assumed lack of
541 organic material in the red colour motifs (Ruiz et al. 2012). In Iberia, radiocarbon dat-
542 ing of sites with post-glacial graphic art has only been achieved for some megaliths,

543 organic matter in black pigments providing chronologies ranging between the 6th and
544 1st millennia BC (Bueno Ramírez et al. 2007). In rock shelters, the importance of red
545 pigments has prompted the use of other techniques such as radiocarbon dating of ox-
546 alate crusts (Ruiz et al. 2012). Congruently with this assumption, U-Th dating of the
547 calcareous crusts grown over the motifs was chosen as a potentially workable dating
548 method. Although some dates congruent with the multi-stratified character of the
549 sample were obtained, they were demonstrated to be doubtful due to its high detrital
550 thorium content. An attempt to TL-date a knapped lithic artefact found in the prox-
551 imities of Matacabras also failed (data not shown). The characterisation of some ce-
552 ramic sherds collected at the surface of Matacabras and the neighbouring site of Pie-
553 dras Blancas I, however, does point out towards a very similar technological and cul-
554 tural background for both sites. Ceramics from both sites point to the use of calcite
555 rich raw materials and low firing temperatures. Nevertheless, one ceramic sherd from
556 Piedras Blancas I has a different composition, pointing to the use of non-carbonated
557 and mafic raw materials.

558

559 Although none of this evidence secures a numerical date for the paintings themselves,
560 it does throw some light onto the chrono-cultural context of the shelter's use and oc-
561 cupation. Relative dating based on the stylistic characteristics of the Matacabras motifs
562 is an alternative resource. A very wide chronological framework is considered for Ibe-
563 rian schematic rock art: from the Early Neolithic to a late imprecise chronology that
564 can reach historical times. The concept of schematic rock art is in itself clearly an artifi-
565 cial category. In fact, different phases of use in panels have started to be noted – and
566 connected with the biographies of these sites - including Palaeolithic and Post-
567 Palaeolithic art as well as much later, 'Protohistoric' art (Royo Guillén 2015, Luis 2009).
568 In addition, recent research has identified schematic rock art in northern and western
569 regions of Iberia, where it had not been recorded before (Sanchez 2016, Figueiredo et
570 al. 2015, Bueno-Ramírez et al. 2016). Indeed, within the schematic rock art phenome-
571 non different nuclei coexist which share a "family resemblance" (Acosta Martínez
572 1968) such as for example La Alcudia valley and Sierra Madrona mountain range (Ciu-
573 dad Real) (Fernández Rodríguez 2003) or La Janda (Cádiz) (Mas Cornellà 2005). These
574 probably have chrono-cultural connotations but the scarcity of absolute dates has not
575 enabled them to be defined. In this sense, Juan Vicent García (2008) notes the existing
576 tendency in this field to repeatedly try to answer the same questions regarding the
577 symbolic and artistic aspects of Neolithic material culture (the research agenda).

578

579 Following Acosta Martínez (1995), the presence of a big pectiniform element and at
580 least two anthropomorphic figures would typologically characterize the Matacabras
581 rock art as belonging to the Middle Neolithic. Nevertheless, the existence of an impor-
582 tant Early Neolithic habitat at El Toro cave (located in El Torcal karstic landscape) in
583 which there is evidence of the use of schematic art on a human skull (Guijo Mauri
584 2004: 289) and the 'ancient style', perceived in some elements of the composition
585 (such as the serpentiform lines), could take us even further back in time.

586

587 Thus, although the chronology for neither Matacabras nor Menga has been precisely
588 established due to the significant problems posed by the empirical record, a temporal
589 precedence of the former over the latter seems likely. The data presented here sug-

590 gest that Matacabras could have been painted prior to c. 3800 BC, even though, as has
591 been pointed out, the sample used in the U-Th dating is not entirely reliable. The lim-
592 ited radiocarbon determinations available for Menga suggest it must have already
593 been erected by between c. 3800 and 3600 BC (García Sanjuán and Lozano Rodríguez
594 2016: 8). The chronometric data currently available allows us to consider the possibil-
595 ity that Matacabras could have in fact been in use when the Menga dolmen was
596 erected. Nevertheless, the chronologic relationship between both sites may not neces-
597 sarily be one of simple diachrony (first Matacabras – then, Menga). On the contrary,
598 this relationship could be synchronic in nature - or the shelter could even be subse-
599 quent to the construction of Menga. The view of La Peña from the plain (and from in-
600 side Menga) is so spectacular that it may have been one of the main causes of the
601 dolmen’s anomalous orientation.

602

603 The second chronological challenge to solve is the possible existence of distinct phases
604 of use of the Matacabras shelter. The restrictive scientific policy on rock art painting
605 enforced by Andalusian cultural authorities, in which conservation is prioritised, has
606 prevented us from taking samples of the pigments for their characterization. There-
607 fore, the information we have is essentially incomplete. Nevertheless, we have the
608 analytic information yielded by the colorimetry of the motifs, the qualitative informa-
609 tion obtained through digital image analysis and the visual observation of the pigment
610 application technique to attempt to shed some light on this matter. Apart from the
611 stylistic criteria, knowing the composition of the pictorial ‘recipe’ used can help to ver-
612 ify the existence of different phases in the production of the panels as we know them
613 today. Differences in the composition of prehistoric pigments can be significant in de-
614 termining the distinct phases in the creation of the panels (Rogerio-Candelera 2014).
615 Digital image analysis, on the one hand, has proven to be a useful tool in producing
616 reliable generalizations based on the optical response of different pictorial recipes
617 (Rogerio-Candelera 2014). At Matacabras, the pigment application technique seems to
618 be very similar across the panel, with lines drawn on using the fingertips, all traces be-
619 ing linear and all the pictorial elements of the panel being approximately 1 cm thick.

620

621 Does the absence of significant differences in the optical behaviour of the paint and
622 the technical and stylistic similarity of techniques/styles suggest that Matacabras is a
623 ‘fossilized panel’ (i.e. a painted composition which has not verified incorporations of
624 other painted elements since its creation [*sensu* Martínez García 2004, 2013])?

625

626 No simple answers can be given for these very difficult questions. On the one hand,
627 recent studies have shown that in rock art caves used and re-used over long periods of
628 time the composition of pigments may not have changed much, as is the case of Tito
629 Bustillo, in northern Spain (De Balbín-Behrmann and Alcolea González 2009). On the
630 other hand, the images obtained in this study suggest that the lines of the serpenti-
631 form were not only covered by the crust analysed further below, but also that on the
632 upper part (where they are less visible) they could be over-imposed by a schematic
633 motif (see sampling points 15-16 in Figure 6). Apparently there are also serpentiform
634 lines under the great central pectiniform, but these are even less perceptible (left of
635 sampling point 14 in Figure 6). Together with a style of Palaeolithic reminiscence, these
636 superimpositions suggest the existence of a long sequence of graphic art executed by

637 hunters and gatherers at Lands of Antequera (Bueno Ramírez and De Balbín-Behrmann
638 2016: 472, De Balbín-Behrmann et al 2017).

639

640 Therefore, we must keep an open mind to the possibility that a degree of diachrony
641 existed in the elaboration of the Matababras motifs, including two phases in which the
642 wavy motifs seem to belong to the earlier one (Bueno Ramírez and De Balbín-
643 Behrmann 2016: 472). Only further research, perhaps aided by radiocarbon dating, will
644 help establish this point.

645

646 Finally, it is worth noting that both the information obtained through electronic mi-
647 croscopy and characterization of the organic compounds found in the walls of the shel-
648 ter indicate taphonomic circumstances influenced by the humidity, the proliferation of
649 photosynthetic organisms and atmospheric contamination (which might be related to
650 the existence of a railway nearby since 1869, which once even had had a station near
651 to La Peña). These data are of importance for the future conservation of these impor-
652 tant remains of prehistoric rock art.

653

654 **6. Conclusions**

655

656 The multi-disciplinary study presented in the previous pages has served to accurately
657 define the graphic material of the Matababras rock shelter, which had only been per-
658 functorily described up until now. The data obtained in our study also reveal that a
659 relationship of diachronic precedence between the graphical motifs of the Matababras
660 rock shelter and the construction of Menga is quite possible, although not strictly nec-
661 essary for explaining the peculiar orientation of the great megalith. The 'internal'
662 chronology of the panel is a difficult problem. As we have discussed above, some evi-
663 dence point to a strong stability in the production of the motifs, with similar pigment
664 composition and execution style, while other evidence suggest a possible diachrony,
665 with superimposition of motifs.

666

667 Besides its intrinsic properties, which we have examined in detail, Matababras is of
668 particular relevance due to its geographical position and visual relationship with
669 Menga. In his archaeoastronomy study on prehistoric monuments of the western
670 Mediterranean, Michael Hoskin (2001) had already pointed out Menga's highly un-
671 usual nature in that it does not face sunrise, as is common in southern Iberian mega-
672 liths, although that does not necessarily mean that the orientation is entirely devoid of
673 other kinds of astronomical significance, as it has been claimed (Lozano Rodríguez et
674 al., 2014). Later investigations demonstrated that Menga's axis of symmetry intersects
675 almost precisely with the foot of the rocky cliff which dominates the northern sector of
676 La Peña de los Enamorados, exactly where Matababras is (Figure15). This characteristic
677 confers an unusual relevance to Matababras in term of the design and biography of
678 this great megalithic monument (García Sanjuán and Wheatley 2010: 22-31, García
679 Sanjuán and Lozano Rodríguez 2016: 7-8). In fact, fieldwork carried out in 2006 and
680 2013 has shown intense Late Neolithic and perhaps (although to a lesser extent), Cop-
681 per Age activity at Piedras Blancas I, located right below Matababras. A significant
682 amount of surface material attributable to these periods has been found at Piedras
683 Blancas I, as well as some monolithic blocks described as possible menhirs (García San-

684 juán and Wheatley 2009, 2010, Bueno Ramírez *et al.* 2009: 188, García Sanjuán *et al.*
685 2015). Also, there is a probable small, megalithic tomb named Piedras Blancas II (Gar-
686 cía Sanjuán and Wheatley 2009: 139).The rock art shelter of Matababras, therefore,
687 was far from isolated on its La Peña location: a major locus of activity, including possi-
688 bly megalithic monuments, was connected to it.

689

690 In addition, Lands of Antequera houses a major series of locations with schematic rock
691 art (Figures 16 and 17) which, having already been discovered and described, await
692 high-resolution studies similar to the one presented here. An interesting aspect of this
693 set of rock art sites is the frequency of panels with Palaeolithic and Post-Palaeolithic
694 sequences, both inside caves and in the open-air. The Palaeolithic serpentiforms of La
695 Pileta and Ardales caves are closely connected to those of Matababras and the Cueva
696 Alta shelter in Cañete la Real. The latter two are located right on natural fissures that
697 accentuate the topographical prominence and visibility of the sites (De Balbín-
698 Behrmann *et al.* 2017:127). Another interesting aspect is the relationship between
699 painting and engraving at some sites, which is generally not very frequent in Iberian
700 schematic rock art (Bueno Ramírez *et al.* 2009). In addition, we must note that the mo-
701 tifs present in the region, even if fitting within the 'classic' repertoire of schematic rock
702 art, show local idiosyncrasies such as the pectiniforms. At La Pileta, a direct radiocar-
703 bon chronology of the first half of the 3rd millennium BC was obtained on a black
704 pectiniform (Sanchidrián Torti *et al.* 2001), thus showing a Palaeolithic/Post-
705 Palaeolithic sequence of interest for Matababras.

706

707 In summary, both landscape and long-term biography are elements clearly embedded
708 in the fabric of Antequera's outstanding megaliths, to an extent rarely seen in other
709 prehistoric monuments worldwide. Regardless of its limited conservation, the graphi-
710 cal motifs of the Matababras rock shelter wonderfully illustrate the complex concep-
711 tual relationship that Neolithic societies established between certain conspicuous
712 natural formations, graphical signs and 'monumental' natural formations. The visual
713 association between Menga and Matababras is unique in Iberia and most probably also
714 in Europe. The future excavation of Matababras and the key site of Piedras Blancas I,
715 which is intrinsically associated with it, will enable us to shed more light on the com-
716 plex conceptual, visual and graphic relationships underlying one of the most complex
717 megalithic landscapes in the world.

718

719 ***Acknowledgements***

720

721 This study has been funded by the project of "Nature, Society and Monumentality:
722 High Resolution Archaeological Investigations on the Megalithic Landscape of Antequera"
723 (HAR2013-45149-P) (2014-2017), sponsored within the National R&D Plan of
724 the Ministry of Economy and Competitiveness (Spanish Government). It has also been
725 carried out within the project "Societies, Territories and Landscapes in the Prehistory
726 of Antequera (Málaga)" (2013-2018), approved by the Ministry of Culture of the Anda-
727 lusanian Government.C2TN/IST authors also gratefully acknowledge the FCT support
728 through the UID/Multi/04349/2013 project.

729

730 ***Bibliographic References***

731
732 Acosta Martínez, P., 1968. La Pintura Rupestre Esquemática en España. Salamanca,
733 Universidad de Salamanca.
734
735 Acosta Martínez, P., 1995. Las culturas del neolítico y calcolítico en Andalucía Occiden-
736 tal. Espacio, Tiempo y Forma, Serie I, Prehistoria y Arqueología 8, 33-80.
737
738 Aranda Jiménez, G., García Sanjuán, L., Mora Molina, C., Moreno Escobar, M.C., Ri-
739 quelme Cantal, J.A., Robles Carrasco, S., Vázquez Paz, J., 2015. Evidencias de asen-
740 tamiento y prácticas funerarias en los dólmenes de Menga y Viera en la Antigüedad. La
741 Intervención de 1988. Menga. Revista de Prehistoria de Andalucía 6:253-289.
742
743 Biscaye, P.E., 1965. Mineralogy and sedimentation of recent deep-sea clay in the Atlan-
744 tic Ocean and adjacent seas and oceans. Geological Society of America Bulletin 76:803-
745 832.
746
747 Bradley, R., García Sanjuán, L., 2017. Sudden Time? Natural disasters as a stimulus to
748 monument building: From Silbury Hill (Great Britain) to Antequera (Spain). In: Bickle,
749 P., Cummings, V., Hofmann, D., Pollard, J., (Eds.), Neolithic Europe: Essays in Honour of
750 Professor Alasdair Whittle. Oxbow, Oxford, pp. 181-201.
751
752 Bueno Ramírez, P., De Balbín-Behrmann, R., 2009. Marcadores gráficos y territorios
753 tradicionales en la prehistoria de la Península Ibérica. Cuadernos de Prehistoria y Ar-
754 queología de la Universidad de Granada 19:65-100.
755
756 Bueno Ramírez, P., De Balbín Behrmann, R., 2016. De cazadores a productores: Transi-
757 ciones y tradiciones. In: Del Neolítico a l'Edat del Bronze en el Mediterrani Occidental:
758 Estudis en Homenatge a Bernat Martí Oliver, TV SIP 119, València, pp. 465-480.
759
760 Bueno Ramírez, P., De Balbín-Behrmann, R., Barroso Bermejo, R., 2007. Chronologie de
761 l'art mégalithique ibérique: C14 et contextes archéologiques. L'Anthropologie 111:590-
762 654.
763
764 Bueno Ramírez, P., De Balbín Behrmann, R., Barroso Bermejo, R., 2009. Análisis de las
765 grafías megalíticas de los Dólmenes de Antequera y su entorno. In: Ruíz González, B.
766 (Ed.), Dólmenes de Antequera: Tutela y Valorización Hoy. Sevilla, Junta de Andalucía,
767 pp. 186-197.
768
769 Bueno Ramírez, P., De Balbín Behrmann, R., Barroso Bermejo, R., 2016. Graphic Holo-
770 cene expressions on the Atlantic façade: Portugal. In: Soares, J. (Ed.), Social Complexity
771 in a Long Term Perspective. Setúbal Arqueológica 16, pp. 41-64.
772
773 Bueno Ramírez, P., De Balbín Behrmann, R., Barroso Bermejo, R., 2018. Steles, time
774 and ancestors in the megaliths of Antequera, Málaga, Spain. Menga. Revista de Prehis-
775 toria de Andalucía 8:167-193
776

777 Cantalejo Duarte, P., Espejo Herrerías, M.M., Cabello Ligeró, L., Becerra Martín, S.,
778 Medianero Soto, J., Aranda Cruces, A., Mora Domínguez, J. 2010. Sobre los antropo-
779 morfos esquemáticos en Málaga: reflejo de unos grupos sociales que mantuvieron un
780 arte subjetivo. In: Martínez García, J., Hernández Pérez, M.S. (Eds.), Actas del II Con-
781 greso de Arte Rupestre Esquemático en la Península Ibérica. Comarca de Los Vélez,
782 Almería, pp. 67-79.
783

784 Cheng H., Edwards, R.L., Shen C.-C., Polyak, V.J., Asmerom, Y., Woodhead, J., Hell-
785 strom, J., Wang, Y., Kong, X., Spötl, C., Wang, X., Alexander, C., 2013. Improvements in
786 ²³⁰Th dating, ²³⁰Th and ²³⁴U half-life values, and U-Th isotopic measurements by multi-
787 collector inductively coupled plasma mass spectrometry. Earth and Planetary Science-
788 Letters 371–372, 82–91.
789

790 Cisneros Franco, J., Corrales Aguilar, M., 1994. Informe sobre la necrópolis de La Angos-
791 tura (Antequera, Málaga). Análisis altimétrico, planimétrico y orientación de los enter-
792 ramientos excavados. Actas del II Congreso Andaluz de Estudios Clásicos, III, So-
793 ciedadde Estudios Clásicos, Málaga, pp. 279-283.
794

795 Daily, M., 1983. Hue-Saturation-Intensity Split-Spectrum processing of Seasat Radar
796 imagery. Photogrammetric Engineering and Remote Sensing 49(3):349-355.
797

798 De Balbín-Behrmann, R., Alcolea González, J.J., 2009. Les colorants de l'art paléolithi-
799 que dans les grottes et en plein air. L'Anthropologie 113, 559-601.
800

801 De Balbín-Behrmann, R., Bueno Ramírez, P., Barroso Bermejo, R., Villanueva Ortíz, P.,
802 2017. Images of the Past in the Lands of Antequera, Málaga, Spain: Palaeolithic to
803 Post-Palaeolithic Transition in Southern Europe. Munibe Antropologia-Arkeologia 68:
804 115-133.
805

806 De la Rosa, J.M., López Capel, E., González-Vila, F.J., González-Pérez, J.A., Manning,
807 D.A.C., 2008. Direct detection of black carbon in soils by Py-GC/MS, ¹³C NMR spectroscopy
808 and thermogravimetric techniques. Soil Science Society of America Journal
809 72:258-267.
810

811 De la Rosa, J.M., Faria, S.R., Varela, M.E., Knicker, H., González-Vila, F.J., González-
812 Pérez, J.A., Keizer, J., 2012. Characterization of wildfire effects on soil organic matter
813 using analytical pyrolysis. Geoderma 191: 24-30.
814

815 De la Rosa J.M., Miller A.Z., Pozo-Antonio J.S., González-Pérez J.A., Jiménez-Morillo
816 N.T., Dionisio A., 2017. Assessing the effects of UVA photocatalysis on soot-coated TiO₂-
817 containing mortars. Science of the Total Environment 605-606, 147-157.
818

819 Dias, M.I., Prudêncio, M.I., Valera, A.C., 2017. Provenance and circulation of Bell Beak-
820 ers from Western European societies of the 3rd millennium BC: The contribution of
821 clays and pottery analyses. Applied Clay Science 146, 334-342.
822

823 Dias, M.I., Prudêncio, M.I., Matos, M.A., Rodrigues, A.L., 2013. Tracing the origin of
824 blue and white Chinese Porcelain ordered for the Portuguese market during the Ming
825 dynasty using INAA. *Journal of Archaeological Science* 40 (7), 3046-3057.

826

827 Dias, M.I., Prudêncio, M.I., Gouveia, M.A., Trindade, M.J., Marques, R., Franco, D., Ra-
828 poso, J., Fabião, C.S., Guerra, A., 2010. Chemical tracers of Lusitanian amphorae kilns
829 from the Tagus estuary (Portugal). *Journal of Archaeological Science* 37, 784-798.

830

831 Díaz-Zorita Bonilla, M., García Sanjuán, L., 2012. Las inhumaciones medievales del atrio
832 del dolmen de Menga (Antequera, Málaga): estudio antropológico y cronología abso-
833 luta. *Menga. Revista de Prehistoria de Andalucía* 3:237-250.

834

835 Elias, M., Chartier, C., Prévot, G., Garay, H., Vignaud, C., 2006. The colour of ochres
836 explained by their composition. *Materials Science and Engineering B* 127, 70-80.

837

838 Fernandes, P., 2006. Applied microbiology and biotechnology in the conservation of
839 stone cultural heritage materials. *Applied Microbiology and Biotechnology* 73, 291-
840 296.

841

842 Fernández Rodríguez, M., 2003. Las Pinturas Rupestres Esquemáticas del Valle de Al-
843 cudia y Sierra Madrona. Mancomunidad de Municipios del Valle de Alcudia y Sierra
844 Madrona, Ciudad Real.

845

846 Figueiredo, S.S., Xavier, P., Silva, A., Neves, D., Dominguez Garcia, I., 2015. The
847 Holocene transition and post-palaeolithic rock art from de Sabor valley (Tras-Os-
848 Montes, Portugal). In: Medina-Alcaide, M.A., Romero Alonso, A.J., Ruiz-Márquez, R.M.,
849 Sanchidrián Torti, J.L. (Eds.) *Sobre Rocas y Huesos: Las Sociedades Prehistóricas y sus*
850 *Manifestaciones Plásticas*. Córdoba, Universidad de Córdoba, pp. 192-203

851

852 García Sanjuán, L., Lozano Rodríguez, J.A., 2016. Menga (Andalusia, Spain): biography of
853 an exceptional megalithic monument. In: Laporte, L., Scarre, C. (Eds.). *The Megalithic*
854 *Architectures of Europe*. Oxford, Oxbow, pp. 3-16.

855

856 García Sanjuán, L., Wheatley, D.W., 2009. El marco territorial de los Dólmenes de
857 Antequera: valorización preliminar de las primeras investigaciones, In: Ruiz González, B.
858 (Ed.). *Dólmenes de Antequera: Tutela y Valorización Hoy*. Sevilla, Junta de Andalucía,
859 pp. 128-143.

860

861 García Sanjuán, L., Wheatley, D., 2010. Natural substances, landscape forms, symbols
862 and funerary monuments: elements of cultural memory among the Neolithic and Cop-
863 per Age societies of Southern Spain. In: Lillios, K., Tsamis, V. (Eds.), *Material Mnemon-*
864 *ics: Everyday Memory in Prehistoric Europe*. Oxford, Oxbow, pp. 10-39.

865

866 García Sanjuán, L., Wheatley, D.W., Díaz-Guardamino Uribe, M., Mora Molina, C.,
867 Sánchez Liranzo, O., Strutt, K., 2015. Evidence of Neolithic activity at La Peña de los En-
868 amorados (Antequera, Málaga): intensive surface survey, geophysics and geoarchaeol-

869 ogy at the site of Piedras Blancas I. Menga. *Revista de Prehistoria de Andalucía* 6, 211-
870 252.

871

872 García Sanjuán, L., Aranda Jiménez, G., Carrión Méndez, F., Mora Molina, C., Lozano
873 Medina, Á., García González, D., 2016. El relleno del pozo de Menga: Estratigrafía y
874 radiocarbono. *Revista de Prehistoria de Andalucía* 7, 199-223.

875

876 Gillespie, A.R., Kahle, A.B., Walker, R.E., 1986. Color enhancement of highly correlated
877 images. I. Decorrelation and HSI contrast stretches. *Remote Sensing of Environment*
878 22, 343-365.

879

880 Gomes, H., Collado, H., Martins, A., Nash, G.H., Rosina, P., Vaccaro, C., Volpe, L., 2015.
881 Pigment in western Iberian schematic rock art: an analytical approach. *Mediterranean*
882 *Archaeology and Archaeometry* 15 (1), 163-175.

883

884 Gorbushina, A.A., 2007. Life on the rocks. *Environmental Microbiology* 9, 1613-1631.

885

886 GozalbesC ravioto, M., 1986. *Las Vías Romanas de Málaga*. Madrid, Colegio de In-
887 genieros de Caminos, Canales y Puertos.

888

889 Guarnido Olmedo, V., 1977. La Depresión de Antequera. *Cuadernos Geográficos de la*
890 *Universidad de Granada* 7, 39-69.

891

892 Guijo Mauri, J.M., 2004. Paleoantropología. In: Martin Socas, D., Camalich Massieu, D.,
893 González Quintero, P. (Eds.). *La Cueva de El Toro (Sierra de El Torcal, Antequera,*
894 *Málaga). Un Modelo de Ocupación Ganadera en el Territorio Andaluz entre el VI y el II*
895 *Milenios ANE*. Sevilla, Junta de Andalucía, pp. 287-290.

896

897 Hermosin, B., Gaviño, M., Saiz-Jimenez, C., 2004. Organic compounds in black crusts
898 from different European monuments: a comparative study. In: Saiz-Jimenez, C. (Ed.).
899 *Air Pollution and Cultural Heritage*. Rotterdam, A.A. Balkema, pp: 47-55.

900

901 Hoffmann, D.L., Prytulak, J., Richards, D.A., Elliot, T., Coath, C.D., Smart, P.L., Scholz, D.,
902 2007. Procedures for accurate U and Th isotope measurements by high precision MC-
903 ICPMS. *International Journal of Mass Spectrometry* 264:97–109.

904

905 Hoffmann, D.L., Pike, A.W.G., García-Diez, M., Pettitt, P.B., Zilhão, J., 2016. Methods for
906 U-series dating of CaCO₃ crusts associated with Palaeolithic cave art and application to
907 Iberian sites. *Quaternary Geochronology* 36:104–119.

908

909 Horwitz, E.P., Dietz, M.L., Chiarizia, R., Diamond, H., 1992. Separation and preconcen-
910 tration of uranium from acidic media by extraction chromatography. *Analytica Chimica*
911 *Acta* 266:25–37.

912

913 Hoskin, M., 2001. *Tombs, Temples and Their Orientation. A New Perspective on Medi-*
914 *terranean Prehistory*. Oxford, Ocarina Books.

915

916 Jaffey, A.H., Flynn, K.F., Glendenin, L.E., Bentley, W.C., Essling, A.M., 1971. Precision
917 measurement of half-lives and specific activities of U²³⁵ and U²³⁸. *Physical Review C* 4,
918 1889-1906.

919

920 Jiménez Aguilera, F., 2006. Archidona. La leyenda de la Peña de los Enamorados.
921 Rayya. *Revista Cultural de la Comarca Norte de Málaga* 2, 11-28.

922

923 Lozano Rodríguez, J.A., Ruiz-Puertas, G. Hódar-Correa, M., Pérez-Valera, F., Morgado
924 Rodríguez, A., 2014. Prehistoric engineering and astronomy of the great Menga Dol-
925 men (Málaga, Spain). A geometric and geoarchaeological analysis. *Journal of Archaeo-
926 logical Science* 41, 759-771.

927

928 Luis, L., 2009. Rock art as landart. A diachronic view of the Coa valley (NE Portugal).
929 Post-Palaeolithic rock art. In De Balbín-Behrmann, R., Bueno-Ramírez, P., González-
930 Antón, R., Del Arco Aguilar, C. (Eds.): *Grabados Rupestres de la Fachada Atlántica Eu-
931 ropea y Africana*. BAR 2043. Oxford, Archaeopress, pp.129-147.

932

933 Martínez García, J., 2004. Pintura rupestre esquemática: una aproximación al modelo
934 antiguo (neolitización) en el Sur de la Península Ibérica. In: *II Simposio de Prehistoria
935 Cueva de Nerja*. Nerja, Fundación Cueva de Nerja, pp. 102-144.

936

937 Martínez García, J., 2013. Pintura rupestre esquemática en los Tajos de Lillo (Loja, Gra-
938 nada) y el modelo antiguo del Arte Esquemático. In: Martínez García, J., Hernández
939 Pérez, M. S. (Eds.), *Arte Rupestre Esquemático en la Península Ibérica*. Actas del II Con-
940 greso (Comarca de los Vélez, Almería, 5-8 de Mayo de 2010), pp. 89-103.

941

942 Martínez-Sevilla, F., Morgado, A., Jiménez Cobos, F., Gutiérrez Rodríguez, M., López
943 García, A., Lozano Rodríguez, J.A. Carrasco Rus, J., 2016. Knapping methods and tech-
944 niques in the bracelets quarry of Cortijo Cevico (Loja, Granada). *Journal of Lithic Stud-
945 ies* 3 (2).

946

947 Mas Cornellà, M. (2005). *La Cueva del Tajo de las Figuras*. Madrid, UNED.

948

949 Márquez Romero, J.E., Fernández Ruiz, J., 2009. *Dólmenes de Antequera. Guía Oficial
950 del Conjunto Arqueológico*. Sevilla, Junta de Andalucía.

951

952 Maura Mijares, R., 2003. Valoración del fenómeno esquemático en el arte prehistórico
953 de Málaga. In: *Actas del II Congreso de Paleontología Villa de Estepona. Paleoantro-
954 pología y Prehistoria*. Pliocénica 3, pp.131-138.

955

956 Maura Mijares, R., 2005. *Las Manifestaciones Rupestres Prehistóricas en las Cuencas
957 de los Ríos Turón y Guadalteba, Málaga*. PhD Thesis, Madrid, UNED.

958

959 Maura Mijares, R., 2011. *Arte Prehistórico en las Tierras de Antequera*. Sevilla, Junta de
960 Andalucía.

961

962 Maura Mijares, R., Recio Ruiz, A., Cantalejo Duarte, P., Aranda Cruces, P., Pérez Gon-
963 zález, J., 2007. Pinturas y grabados rupestres prehistóricos en el abrigo de la Hoya de
964 Archidona, Málaga. *Rayya. Revista cultural de la comarca norte de Málaga* 3, 11-23.
965

966 Meyer, C., Gaspar, D., 2017. Geoposicionamiento, fotogrametría y prospecciones con
967 georradar en el Parque del Olivar del Zaudín, Tomares (Sevilla). In: Vázquez Paz, J., Gar-
968 rido González, P. (Eds.), *El Tesoro de Zaudín: Contextualización Arqueológica del Con-
969 junto Numismático Tardoantiguo de Tomares (Sevilla)*. Sevilla, Junta de Andalucía, pp.
970 189-200.
971

972 Moldoveanu, S.C., 2010. Pyrolysis of organic molecules with applications to health and
973 environmental issues. *Techniques and Instrumentation in Analytical Chemistry* 28, 1-
974 724.
975

976 Montana, G., Randazzo, L., Oddo, I.A., Valenza, M., 2008. The growth of “black crusts”
977 on calcareous building stones in Palermo (Sicily): a first appraisal of anthropogenic and
978 natural sulphur sources. *Environmental Geology* 56, 367–380.
979

980 Moreno Aragüez, A., Ramos Muñoz, J., 1983. La Peña de los Enamorados. Un ya-
981 cimiento de la Edad del Bronce en la Depresión de Antequera. *Mainake* 4-5, 53-74.
982

983 Morgado Rodríguez, A., Lozano Rodríguez, J.A., Pelegrin, J., 2011. Las explotaciones
984 Prehistóricas del sílex de la Formación Milanos (Granada, España). *Menga. Revista de
985 Prehistoria de Andalucía* 2, 135-155.
986

987 Morgado Rodríguez, A., Lozano Rodríguez, J.A., 2011. La explotación prehistórica de
988 afloramientos de rocas ofíticas del sector oriental del Trías de Antequera (España): un
989 patrimonio natural y cultural a valorar y proteger. In: Peinado, A. (Ed.), *Actas del I Con-
990 greso Internacional El Patrimonio Cultural y Natural como Motor de Desarrollo: Inves-
991 tación e Innovación*. Universidad Internacional de Andalucía, Jaén, pp. 1503-1517.
992

993 Muñoz Vivas, V.E., 1991. Las manifestaciones pictóricas del abrigo Cortijo la Escar-
994 dadera. *Zephyrus* 44, 497-510.
995

996 Ordóñez, S., Fort, R., GarcíadelCura, M.A., 1997. Pore size distribution and the durabil-
997 ity of a porous limestone. *Quarterly Journal of Engineering Geology* 30, 221-230.
998

999 Papida S., Murphy W., May E., 2000. Enhancement of physical weathering of building
1000 stones by microbial populations. *International Biodeterioration & Biodegradation* 46,
1001 305-317.
1002

1003 Pereira de Oliveira, B., De la Rosa, J.M., Miller, A.Z., Saiz-Jimenez C., Gómez-Bolea, A.,
1004 Sequeira Braga, M.A., Dionísio, A. 2011. An integrated approach to assess the origins of
1005 black films on a granite monument. *Environmental Earth Sciences* 63, 1677-1690.
1006

- 1007 Pike, A.W.G., Hoffmann, D.L., García-Diez, M., Pettitt, P.B., Alcolea, J., De Balbín, R.,
1008 Gonzalez Sainz, C., De Las Heras, C., Lasheras, J.A., Montes, R., Zilhão, J. 2012. U-
1009 Seriesdating of Paleolithic art in 11 caves in Spain. *Science* 336, 1409–1413.
1010
- 1011 Portillo, M.C., Rogerio-Candelera, M.A., González, J.M., Saiz-Jiménez, C., 2008. Estudios
1012 preliminares de la diversidad microbiana y análisis de imagen de las manifestaciones
1013 parietales de los abrigos de Fuente del Trucho y de Muriecho L (Colungo, Huesca).
1014 In: Rovira Llorens, S., García-Heras, M., Gener, M., Montero-Ruiz, I. (Eds.), *Actas del VII*
1015 *Congreso Ibérico de Arqueometría*. Madrid, pp. 97-107.
1016
- 1017 Prudêncio, M.I., Dias, M.I., Gouveia, M.A., Marques, R., Franco, D., Trindade, M.J.,
1018 2009. Geochemical signatures of Roman amphorae produced in the Sado River estuary,
1019 Lusitania (Western Portugal). *Journal of Archaeological Science* 36, 873-883.
1020
- 1021 Rivas, T., Pozo, S., Paz, M., 2014. Sulphur and oxygen isotope analysis to identify
1022 sources of sulphur in gypsum-rich black crusts developed on granites. *Science of the*
1023 *Total Environment* 482-483, 137-147.
1024
- 1025 Robert, M., Berthelin, J., 1986. Role of biological and biochemical factors in soil mineral
1026 weathering. In: Huang, P.M., Schnitzer, M. (Eds.), *Interactions of Soil Minerals with*
1027 *Natural Organics and Microbes*. Soil Science Society of America (Special Publ. 17),
1028 Madison (Wi), pp. 452-495.
1029
- 1030 Rodríguez Vinceiro, F.J., Fernández Rodríguez, L.E., Clavero Toledo, J.L., Romero Silva,
1031 C., Von Thode Mayoral, C., García Pérez, A., Suárez Padilla, J., Barrera, M., Palomo La-
1032 buru, A., 1992. Estado actual de la investigación arqueometalúrgica prehistórica en la
1033 provincia de Málaga. *Trabajos de Prehistoria* 49, 217-242.
1034
- 1035 Rogerio-Candelera, M.A., 2014. Propuesta metodológica para establecer la secuencia
1036 estratigráfica de un panel rupestre: La Coquenera II (Obón, Teruel, España). In: Medina-
1037 Alcaide, M.A., Romero Alonso, A.J., Ruiz-Márquez, R.M., Sanchidrián Torti, J.L. (Eds.)
1038 *Sobre Rocas y Huesos: Las Sociedades Prehistóricas y sus Manifestaciones Plásticas*.
1039 Córdoba, Universidad de Córdoba, pp. 330-343.
1040
- 1041 Rogerio-Candelera, M.A., 2015. Digital image analysis based study, recording, and pro-
1042 tection of painted rock art. Some Iberian experiences. *Digital Applications in Archae-*
1043 *ology and Cultural Heritage* 2, 68-78.
1044
- 1045 Rogerio-Candelera, M.A., Élez Villar, J. 2010. Elaboración de un nuevo calco del cáprido
1046 de la Sala de La Hoya (cueva de Altamira) mediante técnicas de análisis de imagen. In:
1047 Saiz, M.E., López, R., Cano, M.A., Calvo, J.C. (Eds.), *Actas del VIII Congreso Ibérico de*
1048 *Arqueometría*. Teruel, SAET, pp. 409-418.
1049
- 1050 Rogerio-Candelera, M.A., Linares Catela, J.A., 2015. El análisis digital de imágenes
1051 como herramienta arqueológica. Estudio de los restos de pintura de los ortostatos del
1052 dolmen 3 de El Pozuelo. In: Moreno Oliva, M., Rogerio-Candelera, M.A., López Navar-

1053 rete, J.T., Hernández Jolín, V. (Eds.), Estudio y Conservación del Patrimonio Cultural.
1054 Málaga, TechnoHeritage/Universidad de Málaga, pp. 82-85.
1055
1056 Rogerio-Candelera, M.A., Figueiredo, S.S., Guimarães, P., Baptista, A.M., 2010. Análisis
1057 de imagen de pinturas rupestres del yacimiento de Faia (Parque Arqueológico de Vila
1058 Nova de FozCôa, Guarda, Portugal). In: Saiz, M.E., López, R., Cano, M.A., Calvo, J.C.
1059 (Eds.), Actas del VIII Congreso Ibérico de Arqueometría. Teruel, SAET, pp. 419-427.
1060
1061 Rogerio-Candelera, M.A., Jurado, V., Laiz, L., Saiz-Jiménez, C., 2011. Laboratory and in
1062 situ assays of digital image analysis based protocols for biodeteriorated rock and mural
1063 paintings recording. *Journal of Archaeological Science* 38, 2571-2578.
1064
1065 Rogerio-Candelera, M.A., Figueiredo, S.S., Borges, A.F., 2013. Cachão da Rapa prehis-
1066 toric rock art paintings revisited: digital image analysis approach for the assessment of
1067 Santos Júnior's tracings. In: Rogerio-Candelera, M.A., Lazzari, M., Cano, E. (Eds.), *Sci-
1068 ence and Technology for the Conservation of Cultural Heritage*. London, CRC Press, pp.
1069 261-264.
1070
1071 Royo Guillén, J.I., 2015. Arte rupestre protohistórico en la cuenca media del Ebro: un
1072 símbolo gráfico de las élites emergentes de la Edad del Hierro. *Cuadernos de Prehis-
1073 toria y Arqueología de Castellón* 33, 97-128.
1074
1075 Ruiz, J.F., Hernanz, A., Armitage, R.A., Rowe, M.W., Viñas, R., Gavira-Vallejo, J.M.,
1076 Rubio, A., 2012. Calcium oxalate AMS 14C dating and chronology of post-Palaeolithic
1077 rock paintings in the Iberian Peninsula. Two dates from Abrigo de los Oculados
1078 (Henarejos, Cuenca, Spain). *Journal of Archaeological Science* 39, 2655-2667.
1079
1080 Saiz-Jimenez, C., Grimalt, J., Garcia-Rowe, J., Ortega-Calvo, J.J., 1991. Analytical pyroly-
1081 sis of lichen thalli. *Symbiosis* 11, 313-326.
1082
1083 Saiz-Jimenez, C., Garcia-Rowe, J., Garcia del Cura, M.A., Roekens, E., van Grieken, R.,
1084 1990. Endolithic cyanobacteria in Maastricht limestone. *Science of the Total Environ-
1085 ment* 94, 209-220.
1086
1087 Saiz-Jimenez, C., Ortega-Calvo, J.J., de Leeuw, J.W., 1995. The chemical structure of
1088 fungal melanins and their possible contribution to black stains in stone monuments.
1089 *Science of the Total Environment* 167, 305-314.
1090
1091 Sanz de Galdeano, C., Lozano Rodríguez, J.A., Puga Rodríguez, E., 2008. El "Trías de
1092 Antequera". *Naturaleza, origen y estructura*. *Revista de la Sociedad Geológica de
1093 España* 21, 3-4.
1094
1095 Sanches, M.J., 2003. Sobre a ocupação do Neolítico Inicial no Norte de Portugal. In:
1096 Gonçalves, V.S.(Ed.), *Muita Gente, Poucas Antas? Origens, Espaços e Contextos do
1097 Megalitismo*. *Trabalhos de Arqueologia* 25, 155-179.
1098

- 1099 Sanches, M.J., 2016. The paintings of “oculadas” figures in the Neolithic and Chalco-
1100 lithic of Northern Portugal: the study case of Serra de Passos. In: FábregasValcarce, R.,
1101 Rodríguez Rellán, C., (Eds.), *Public Images, Private Readings: Multi-Perspective Ap-*
1102 *proaches to the Post-Palaeolithic Rock Art. Proceedings of the XVII UISPP World Con-*
1103 *gress (1–7 September 2014, Burgos, Spain) Volume 5 / Session A11e.* Oxford, Archaeo-
1104 *press*, pp. 50-62.
- 1105
- 1106 Sanchidrian Torti, J.L., Márquez, A.M., Valladas, H., Tisnerat, H. 2001. Dates directes
1107 pour l’Art Rupestre d’Andalousie (Espagne). *International Newsletter on Rock Art* 29,
1108 15-19.
- 1109
- 1110 Sanjurjo Sánchez, J., Trindade, M., Blanco-Rotea, R., Benavides Garcia, R., Fernández-
1111 Mosquera, D., Burbidge, C., Prudêncio, M.I., Dias, M.I., 2010. Chemical and mineralogi-
1112 cal characterization of historic mortars from the Santa Eulalia de Bóveda temple, NW
1113 Spain. *Journal of Archaeological Science* 37(9), 2346-2351.
- 1114
- 1115 Schiavon, N., Chiavari, G., Schiavon, G., Fabbri, D. 1995. Nature and decay effects of
1116 urban soiling on granitic building stones. *Science of the Total Environment* 167, 87-101.
- 1117
- 1118 Sebastián López, M., Palomo Arroyo, M., Rincón Ramírez, J.A., Ormeño Villajos, S.,
1119 Vicent García, J.M., 2013. Métodos de documentación, análisis y conservación no inva-
1120 sivos para el arte rupestre postpaleolítico: radiometría de campo e imágenes multi-
1121 espectrales. *Ensayos en la cueva del Tío Garroso (Alacón, Teruel)*. In: *La Ciencia y el*
1122 *Arte IV. Ciencias Experimentales y Conservación del Patrimonio*. Madrid, Ministerio de
1123 *Educación Cultura y Deporte*, pp. 279-287.
- 1124
- 1125 Standley, L.J., Simoneit, B.R.T., 1987. Characterization of extractable plant wax, resin,
1126 and thermally matured components in smoke particles from prescribed burns. *Envi-*
1127 *ronmental Science & Technology* 21, 163-169.
- 1128
- 1129 Suárez Padilla, J., Fernández Rodríguez, L.E., Rodríguez Venceiro, F.J., Von Thode May-
1130 oral, C., García Pérez, A., Barrera Polo, M., Palomo Laburu, A., 1995. La Peña de los En-
1131 amorados de Antequera (Ladera Oeste). Un importante enclave en la Ruta del Genil
1132 hacia la Andalucía Oriental. In: *Actas del XXI Congreso Nacional de Arqueología (I)*.
1133 *Zaragoza*, pp. 73-84.
- 1134
- 1135 Trindade, M.J., Rocha, F., Dias, M.I., Prudêncio, M.I., 2013. Mineralogy and grain-size
1136 distribution of clay-rich rock units of the Algarve Basin (South Portugal). *Clay Minerals*
1137 48 (1), 59–83.
- 1138
- 1139 Trindade, M.J., Dias, M.I., Rocha, F., Prudêncio, M.I., Coroado, J., 2011. Bromine vola-
1140 tilization during firing of calcareous and non-calcareous clays: Archaeometric implica-
1141 tions. *Applied Clay Science* 53, 489-499.
- 1142
- 1143 Trindade, M.J., Dias, M.I., Coroado, J., Rocha, F., 2010. Firing tests on clay-rich raw ma-
1144 terials from the Algarve Basin (South Portugal): Study of the mineral transformations
1145 with temperature. *Clays and Clay Minerals* 58, 188-204.

1146
1147 Trindade, M.I., Dias, M.I., Coroado, J., Rocha, F., 2009. Mineralogical transformation of
1148 calcareous rich clays with firing: A comparative study between calcite and dolomite
1149 rich clays from Algarve, Portugal. *Applied Clay Science* 42, 345-355.
1150
1151 Vicent García, J.M., 2008. Simbolismo, arte y mundo funerario. In: Hernández Pérez,
1152 M.S., Soler Díaz, J.A., López Padilla, J.A. (Eds.). *Actas del IV Congreso del Neolítico Pen-*
1153 *insular. Tomo II. Alicante, Museo Arqueológico de Alicante*, pp. 11-12.
1154
1155 Wedepohl, K.H., 1995. The composition of the continental crust. *Geochimica et Cos-*
1156 *mochimica Acta* 59, 1217–1232.
1157
1158
1159
1160
1161 **Captions**
1162
1163 **Tables**
1164
1165 Table 1. Correlation coefficients among the bands of image 5260 of Matacabras rock
1166 shelter.
1167
1168 Table 2. Average colorimetric values of the rock support and paint (n=3).
1169
1170 Table 3. U and Th concentrations, isotopic activity ratios and U-Th ages for sample
1171 MC2.
1172
1173 Table 4. Compounds identified by Py-GC/MS.
1174
1175 Table 5. Mineralogical composition obtained by XRD on the non-oriented aggregates of
1176 the bulk sample of the ceramic paste collected at Matacabras and Piedras Blancas I
1177 sites (Spain). Semi-quantification (%) was done by using the diagnostic reflection areas,
1178 considering the full width at half maximum (FWHM) of the main minerals (Sanjurjo
1179 Sánchez et al. 2010; Trindade et al. 2013) and then weighted by empirical factors or
1180 calculated parameters (Biscaye 1965).
1181
1182 Table 6. Concentration of chemical elements obtained by INAA for ceramics of Mata-
1183 cabras and Piedras Blancas I sites (Spain). Major elements (Na₂O, K₂O, Fe₂O₃T) in %
1184 and trace elements in µg/g (ppm).
1185
1186 **Figures**
1187
1188 Figure 1: Location of Matacabras rock art shelter in Iberia (left) and Lands of Antequera
1189 with regards to the Neolithic sites known in the region (right). Design: María del Car-
1190 men Moreno Escobar.
1191

1192 Figure 2A: A) Geological map of the Antequera region showing the location of various
1193 abiotic products used in the Late Prehistory as well as archaeological; Gal: Los Gallum-
1194 bares (Loja, Granada); Rel: Cerro del Reloj (Montefrío, Granada); CV: Cortijo Cevico
1195 (Loja, Granada). 2B) Geological map of La Peña de los Enamorados, where the Mata-
1196 cabras rock art shelter is located. Legend: 1) Triassic (Subbetic (SB); gypsum, clays and
1197 dolomites); 2) Late Jurassic (SB; micrite limestones with oncoliths and pellets); 3) Mid-
1198 dle Jurassic (SB; oolitic limestones); 4) Upper Jurassic (SB; red limestones with nod-
1199 ules); 5) Cretacic – Paleogene (SB; marls and pink limestone marls); 6) Eocene (Flysch;
1200 calcarenites with nummulites); 7) Paleogene (Flysch; brown clays with banks of sand-
1201 stones with quartzs); 8) Pliocene (Breccia cemented with carbonated pebbles); 9) Qua-
1202 ternary (piedmont, hillside deposits); 10) Quaternary (fluvial and flood plain deposits);
1203 a) Minor fault; b) Major fault between domains; c) Concordant normal contact; d) Dis-
1204 cordant contact. Design: José Antonio Lozano Rodríguez.

1205

1206 Figure 3: A) The markedly anthropomorphic silhouette of La Peña de los Enamorados,
1207 as seen from the East. B) Graphic re-creation of the La Peña de los Enamorados legend
1208 published in Basel in 1610 as part of the German edition of the 'Cosmographia Univer-
1209 salis' (first edition 1507). Source: Archive Conjunto Arqueológico Dólmenes de Ante-
1210 quera (CADA).

1211

1212 Figure 4: 3D Views and elevation of the painted area of Matababras shelter. Design:
1213 Diego Gaspar.

1214

1215 Figure 5: Ortophotographic plan of Matababras shelter. Design: Diego Gaspar.

1216

1217 Figure 6: A) Standard RGB frame of a part of the panel. B) Band corresponding to the
1218 third PC. C) ECS stretching in HSI colour space. D) False colour pondering third PC. De-
1219 sign: Miguel Ángel Rogerio-Candelera.

1220

1221 Figure 7: Sampling points for colour measurement over a false colour image obtained
1222 by PCA. Design: Miguel Ángel Rogerio-Candelera.

1223

1224 Figure 8: Sampling points for FESEM and Py-GC/MS. Design: Miguel Ángel Rogerio-
1225 Candelera.

1226

1227 Figure 9: General tracing of the painted panel of Matababras shelter superimposed to
1228 the 3D model of the shelter. Design: Miguel Ángel Rogerio-Candelera and Diego Gas-
1229 par.

1230

1231 Figure 10: MC2 before (a) and after (b) sampling. Dashed black line represents ap-
1232 proximate extent of removed calcite. Design: Alistair Pike and Christopher D. Standish.

1233

1234 Figure 11: FESEM-EDS examinations of the black patina collected from the vertical sur-
1235 face of Matababras Shelter (samples MT1 and MT2). A) General view of sample MT1
1236 showing a discontinuous layer of gypsum crystals. B) Detailed view of gypsum crystals
1237 on MT1 sample. C) EDS spectrum recorded in position 1. D) EDS spectrum recorded in

1238 position 2. E) General view of sample MT2 depicting algal cells and extracellular poly-
1239 meric substances (arrows). F) Diatom cell in sample MT2. Design: Ana Z. Miller.
1240
1241 Figure 12: Pyrochromatogram obtained at 500°C of MT2 sample. Design: José M. De la
1242 Rosa Arranz.
1243
1244 Figure 13: Mineralogical composition obtained by XRD for ceramic samples from Mata-
1245 cabras (CerMC3) and Piedras Blancas I (CerPBI2-1) enhancing the diagnose peaks: PH -
1246 Phyllosilicates; A – Anatase; Q – Quartz; F – Alkalifeldspars; P – Plagioclase; C – Calcite;
1247 H – Hematite. Design: María Isabel Dias and María Isabel Prudêncio.
1248
1249 Figure 14: (A): Tree diagram for Matababras (MC) and Piedras Blancas I (PBI) ceramics
1250 by using the UPGMA (Unweighted pair-group average) as amalgamation (linkage) rule
1251 and the Euclidean distances. Sample CerPBI 1-1 is detachable from all the others. Some
1252 MC and PBI samples have similar chemical composition. (B): Bivariate plot of the sum
1253 of Rare Earth Elements and the sum of the first row transition chemical elements. De-
1254 sign: María Isabel Dias and María Isabel Prudêncio.
1255
1256 Figure 15: Projection of the symmetry axis of Menga Dolmen, intersecting almost ex-
1257 actly with the basement of the rocky wall of the North sector of La Peña de losEnamo-
1258 rados, where Matababras shelter is placed. Design: David W. Wheatley.
1259
1260 Figure 16: Location of Palaeolithic and Post-Palaeolithic rock art sites (shelters and
1261 caves) at Lands of Antequera. Source: De Balbín-Behrmann et al 2007.
1262
1263 Figure 17: Serpentiphorms located at various sites: A) La Pileta cave (Photo: Pedro Can-
1264 talejo Duarte); B) Ardales cave (Photo: Pedro Cantalejo Duarte); C) Laja Alta cave
1265 (Photo: Javier Pérez González); D) Matababras (Photo: Rodrigo de Balbín-Behrmann);
1266 E) Detail of pectiniform at Shelter nº 10 of Las Peñas de Cabrera (Photo: Rodrigo de
1267 Balbín-Behrmann).
1268
1269
1270

Table 1. Correlation coefficients among the bands of image 5260 of Matababras rock shelter.

	PC1	PC2	PC3
PC1	1	0.99089017	0.96449487
PC2	0.99089017	1	0.98718422
PC3	0.96449487	0.98718422	1

Table 2 – Average colorimetric values of the rock support ($n=3$) and paint ($n=3$).

	L*	a*	b*
Stone 1	48.6 ± 10.7 (a)	5.0± 1.2(a)	14.3± 2.1 (a)(b)
Stone 2	58.5 ± 18.3 (a)	4.4 ± 1.3 (a)	14.8 ± 2.8 (a)(b)
Serpentiform 1	50.7 ± 5.5 (a)	16.1± 2.2(b)	11.7 ± 0.6 (a)
Anthropomorph A	57.6 ± 2.3 (a)	10.9± 5.0 (b)	12.9 ± 2.4(a)(b)
Pectiniform	50.4± 6.5 (a)	8.4± 0.9 (c)	11.0± 2.6 (a)
Great pectiniform	59.4± 4.6 (a)	5.9± 2.1 (a)(c)	11.1± 1.3 (a)

Mean values are presented together with the standard deviation (SD) and ANOVA results. Values within each column, followed by the same letters in brackets (a,b, and c) are not significantly different by the Tukey HDS test at $p < 0.05$.

Table 3. U and Th concentrations, isotopic activity ratios and U-Th ages for sample MC2.

Lab ID	Sample ID	^{238}U (ng/g)	\pm	^{232}Th (ng/g)	\pm	$(^{230}\text{Th}/^{232}\text{Th})$	\pm	$(^{230}\text{Th}/^{238}\text{U})$	\pm	$(^{234}\text{U}/^{238}\text{U})$	\pm	Uncorrected Age (ka)	Corrected Age (ka)	Age Error		$(^{234}\text{U}/^{238}\text{U})_{\text{initial}}$	\pm	Minimum Age (ka)
														+	-			
UoS-UTh-A156	MC2a	1088.8	68.1	749.7	46.4	0.9834	0.0105	0.2216	0.0024	1.0379	0.0021	26.14	5.38	12.57	5.06	1.0470	0.0073	0.32
UoS-UTh-A157	MC2b	1020.7	59.3	627.3	36.8	1.0493	0.0107	0.2110	0.0028	1.0424	0.0020	24.63	6.38	11.04	5.90	1.0514	0.0067	0.48
UoS-UTh-A158	MC2c	1266.8	73.4	818.1	48.7	1.3602	0.0129	0.2874	0.0032	1.0431	0.0021	35.07	15.85	11.11	10.03	1.0543	0.0074	5.82

Analytical errors are 2σ of the mean. $(^{230}\text{Th}/^{238}\text{U}) = 1 - e^{-\lambda_{230}T} + (\delta^{234}\text{U}_{\text{measured}}/1000)[\lambda_{230}/(\lambda_{230} - \lambda_{234})](1 - e^{-(\lambda_{230} - \lambda_{234})T})$, where T is the age. Decay constants are $9.1705 \times 10^{-6} \text{ a}^{-1}$ for ^{230}Th , $2.8221 \times 10^{-6} \text{ a}^{-1}$ for ^{234}U (Cheng et al., 2013), and $1.55125 \times 10^{-10} \text{ a}^{-1}$ for ^{238}U (Jaffey et al., 1971).

Table 4. Compounds identified by Py-GC/MS

Peak	Retention time (min)	Compound	%
1	2 071	Acetic acid	1.60
2	2 254	Furan, 2,5-dimethyl-	0.91
3	2 477	Pyridine	1.06
4	2 552	Toluene	4.02
5	2 752	Furfural	1.98
5	2 900	Furfural	5.19
6	3 152	Pyridine, 3-methyl-	3.30
7	3 340	Styrene	1.92
8	3 477	Furan, 2,3, 5-trimethyl-	1.93
9	3 552	2H-Pyran, 3,4-dihydro-	1.39
10	3 735	2(5H)-Furanone, 5-methyl-	1.09
11	3 849	2-Pentanone, 3-methyl-	1.64
12	3 917	2-Furancarboxaldehyde, 5-methyl-	3.43
13	4 095	1-Decene	0.84
14	4 163	Phenol	2.26
15	4 318	Pyridine, 3-methoxy	2.85
16	4 535	Uracil	1.64
17	4 620	2-Cyclopenten-1-one, 2-hydroxy-3-methyl-	1.61
18	4 729	Thiophene, 2-methoxy-5-methyl	2.59
19	5 083	p -Cresol	3.89
20	5 186	2,4,5-Trihydroxypyrimidine	2.21
21	5 552	Maltol	1.27
22	5 781	Benzyl nitrile	1.42
23	6 072	2-Heptenoic acid, methyl ester	1.90
24	6 118	Phenol, 3-ethyl-	1.78
25	6 198	2-Acetamidothiazole	1.02
26	6 261	1-Dodecene	0.92
27	6 501	1,4:3,6-Dianhydro-.alpha.-d-glucopyranose	3.85
27	6 769	1,4:3,6-Dianhydro-.alpha.-d-glucopyranose	0.84
28	6 815	Benzofuran, 2,3-dihydro-	4.45
29	7 009	Benzenepropanenitrile	1.26
30	7 370	Picolinamide	1.13
31	7 478	6-Tridecene	0.78
32	7 735	1H-Indole	1.31
33	8 038	2-Furanmethanol, .alpha.-(2-nitropropyl)-	1.08
34	8 250	Nonane, 2-methyl-3-methylene	0.75
35	8 713	2-Tetradecene, (E)-	0.88
36	8 873	7-Methylindole	1.33
37	9 073	Naphthalene, 2,6-dimethyl-	2.67
38	9 301	Nonanoic acid, methyl ester	1.22
39	9 793	Pyridine, 3-phenyl-	1.79
40	9 924	1-Pentadecene	0.86
41	10 141	1H-Indole, 1,3-dimethyl-	1.97
42	10 382	3-Pyridinecarbothioamide	2.37
43	10 936	Levoglucofan	2.20
44	11 153	Acetylcoumarin	2.58
45	12 233	1-Heptadecene	1.36
46	12 308	Heptadecane	1.72
47	12 650	n-alkyl-pentadecene	0.82
48	13 325	1-Octadecene	0.82
49	13 811	Neophytadiene	1.61
50	13 891	8-Methyloctahydrocoumarin	0.65
51	14 119	1,12-Tridecadiene	0.64
52	14 256	Nonadecane	0.77
53	14 410	Hexadecane, 2,6,10,14-tetramethyl,	0.49
54	15 039	Z-11-Tetradecenoic acid	0.68

55	15 954	unidentified branched n-alkene	0.24
56	16 280	1-Heneicosene	0.41
57	17 171	9-Octadecenamide (Oleic acid amide)	0.25
58	17 560	Diclorodibenzofuran	0.23
59	17 714	9,10-Anthracenedione, 1-amino-4hydroxy-	0.30

Table 5. Mineralogical composition obtained by XRD on the non-oriented aggregates of the bulk sample of the ceramic paste collected at Matababras and Piedras Blancas I sites (Spain). Semi-quantification (%) was done by using the diagnostic reflection areas, considering the full width at half maximum (FWHM) of the main minerals (Sanjurjo Sánchez et al. 2010; Trindade et al. 2013) and then weighted by empirical factors or calculated parameters (Biscaye 1965).

	Phyllosilicates	Quartz	Calcite	Alkali-Feldspars	Plagioclase	Anatase	Hematite	Amphibole
CerMC 2	51	25	9	5	5	5	-	-
CerMC 3	30	31	21	4	5	7	2	-
CerPBI 1-1	45	43	-	-	7	-	3	2
CerPBI 2-1	65	28	-	4	-	3	-	-
CerPBI 2-2	35	30	17	4	4	10	-	-
CerPBI 2-3	55	32	-	6	-	7	-	-
CerPBI 2-4	4	65	7	8	7	3	6	-

Table 6

Table 6. Concentration of chemical elements obtained by INAA for ceramics of Matababras and Piedras Blancas I sites (Spain). Major elements (Na₂O, K₂O, Fe₂O₃T) in % and trace elements in µg/g (ppm).

	CerMC 2	CerMC 3	CerPBI 1-1	CerPBI 2-1	CerPBI 2-2	CerPBI 2-3	CerPBI 2-4
Na₂O	0.47	0.41	0.98	0.47	0.59	0.38	0.60
K₂O	2.41	2.21	1.64	1.98	2.46	2.10	2.32
Fe₂O₃T	7.42	5.35	8.30	7.18	5.07	7.77	5.18
Sc	18.8	13.3	20.5	17.2	12.6	18.3	12.3
Cr	137	77.5	99.9	113	91.7	120	78.8
Co	22.3	18.1	21.3	17.8	15.5	17.6	17.3
Zn	6.63	84.4	132	127	95.3	131	88.8
Ga	17.7	14.7	17.5	19.5	20.0	21.9	18.8
As	4.98	6.85	9.42	7.13	4.87	9.13	7.62
Br	3.19	1.58	3.80	1.39	1.27	2.27	1.20
Rb	66.9	75.6	49.0	61.3	87.5	82.1	95.0
Zr	154	208	190	271	211	224	216
Sb	0.53	0.59	0.65	0.66	0.49	0.50	0.86
Cs	4.58	4.50	2.30	4.63	5.49	5.88	5.67
Ba	559	408	1290	627	322	488	408
La	44.2	35.0	30.1	52.5	34.9	55.4	37.2
Ce	73.4	72.3	58.3	101.0	71.4	88.4	78.7
Nd	34.8	34.9	27.6	45.3	35.3	41.6	33.1
Sm	7.35	6.54	6.45	8.84	6.22	7.96	7.23
Eu	1.43	1.25	1.32	1.75	1.25	1.73	1.33
Tb	1.07	0.83	1.06	1.14	0.65	1.32	0.97
Yb	2.76	2.68	2.65	3.31	2.40	3.29	3.04
Lu	0.26	0.13	0.40	0.52	0.42	0.52	0.44
Hf	4.33	4.79	3.77	6.88	4.46	5.84	5.87
Ta	1.44	1.13	1.04	1.74	1.17	1.85	1.26
Th	11.9	9.95	13.2	13.4	9.79	14.6	11.2
U	1.37	1.63	1.82	2.65	4.74	2.32	2.26

Figure 1
[Click here to download high resolution image](#)

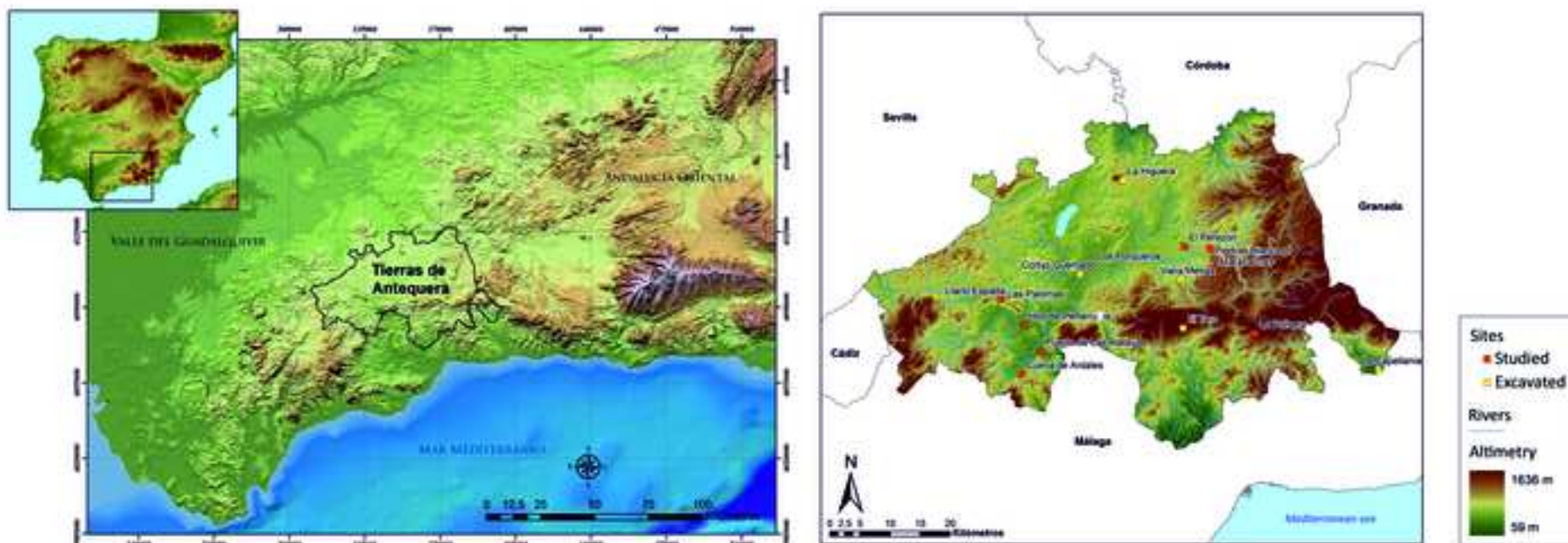


Figure 2

[Click here to download high resolution image](#)

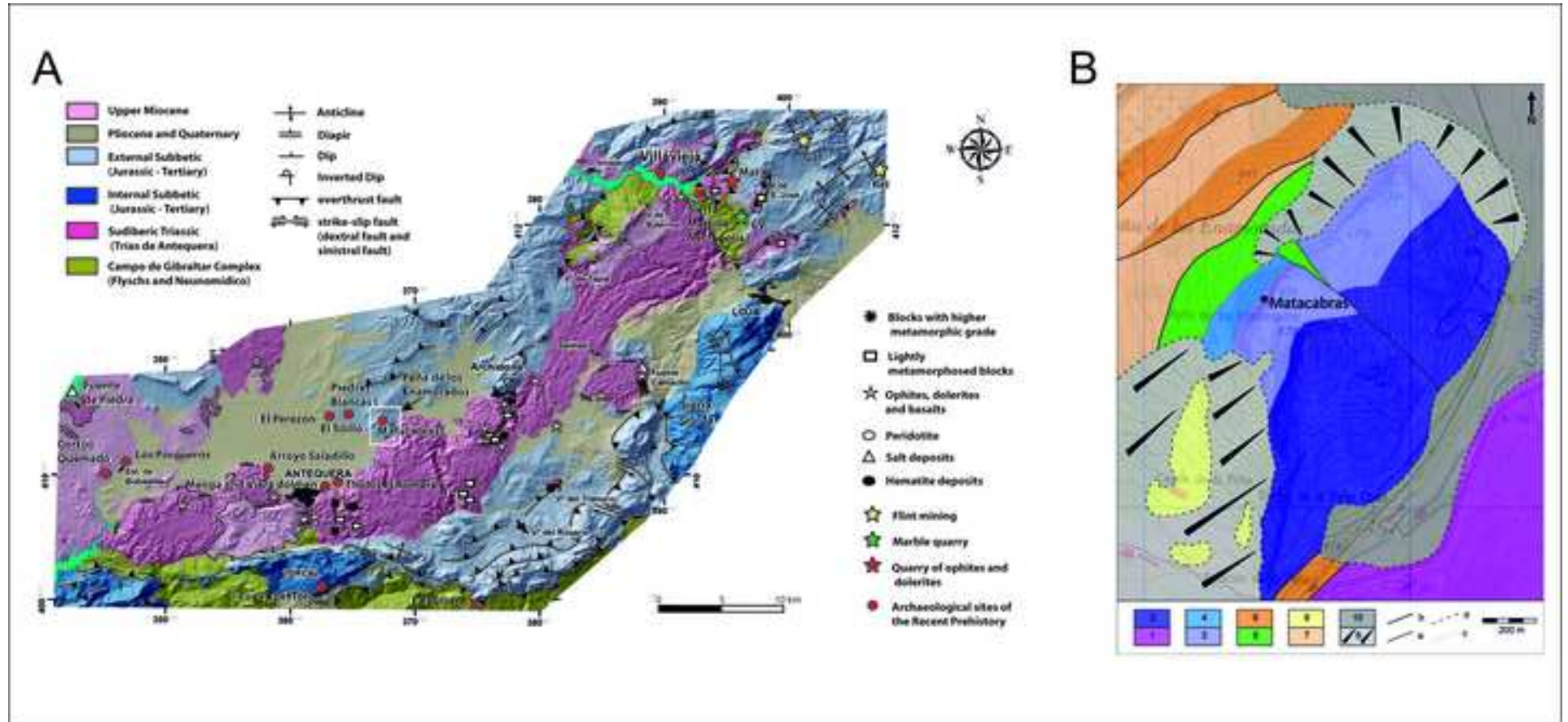


Figure 3
[Click here to download high resolution image](#)



Figure 4

[Click here to download high resolution image](#)

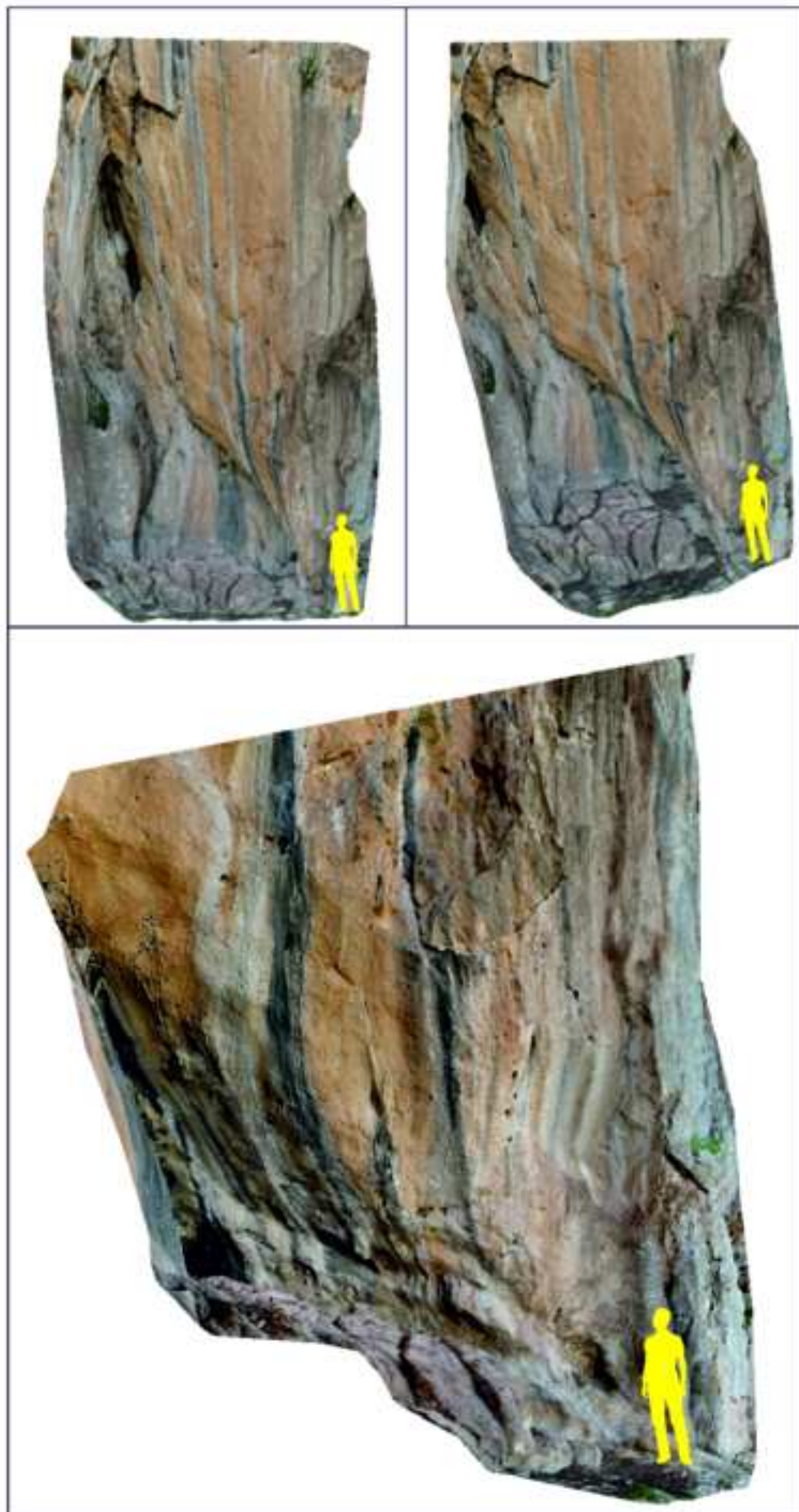


Figure 5
[Click here to download high resolution image](#)

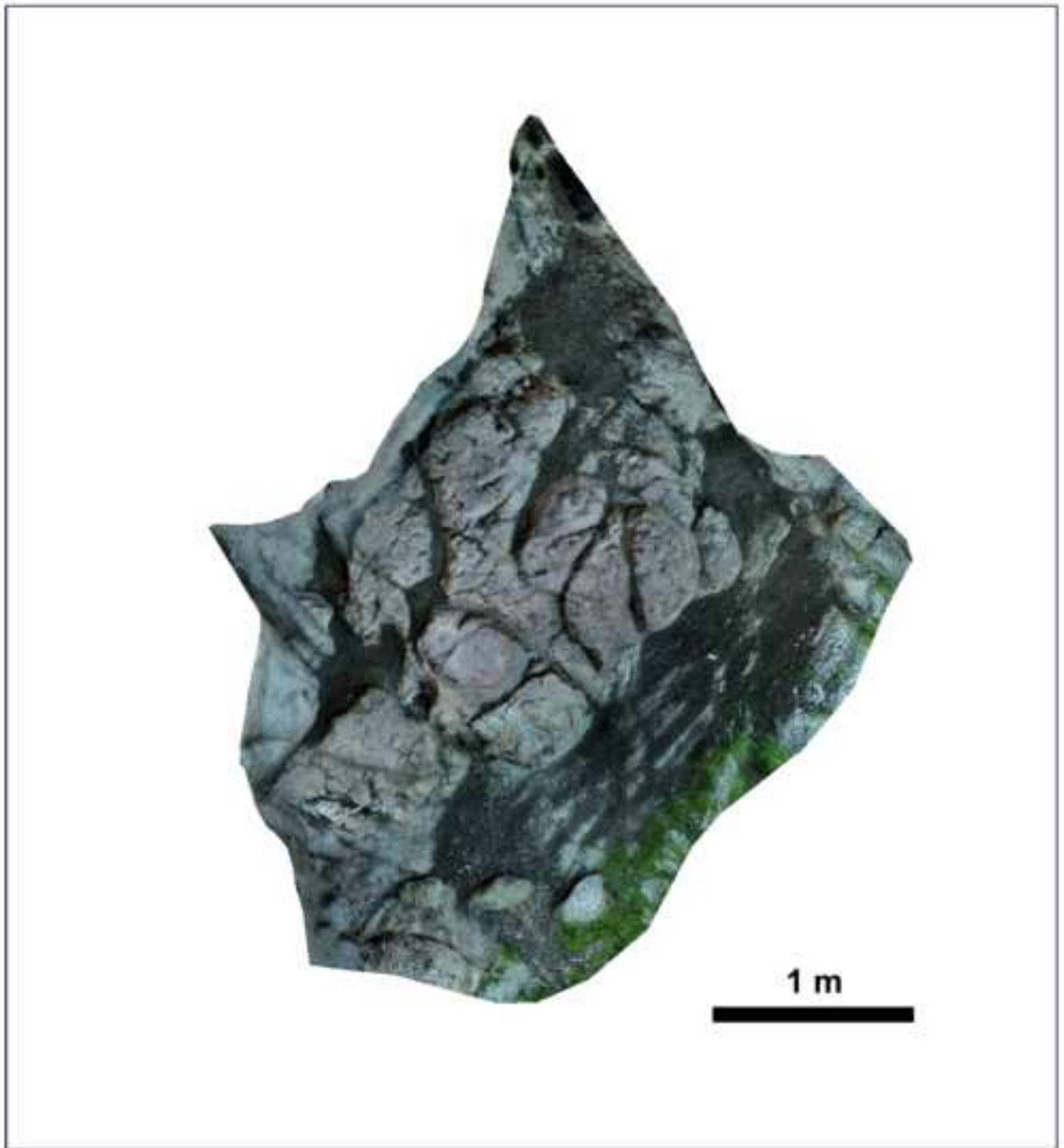


Figure 6
[Click here to download high resolution image](#)



Figure 7

[Click here to download high resolution image](#)

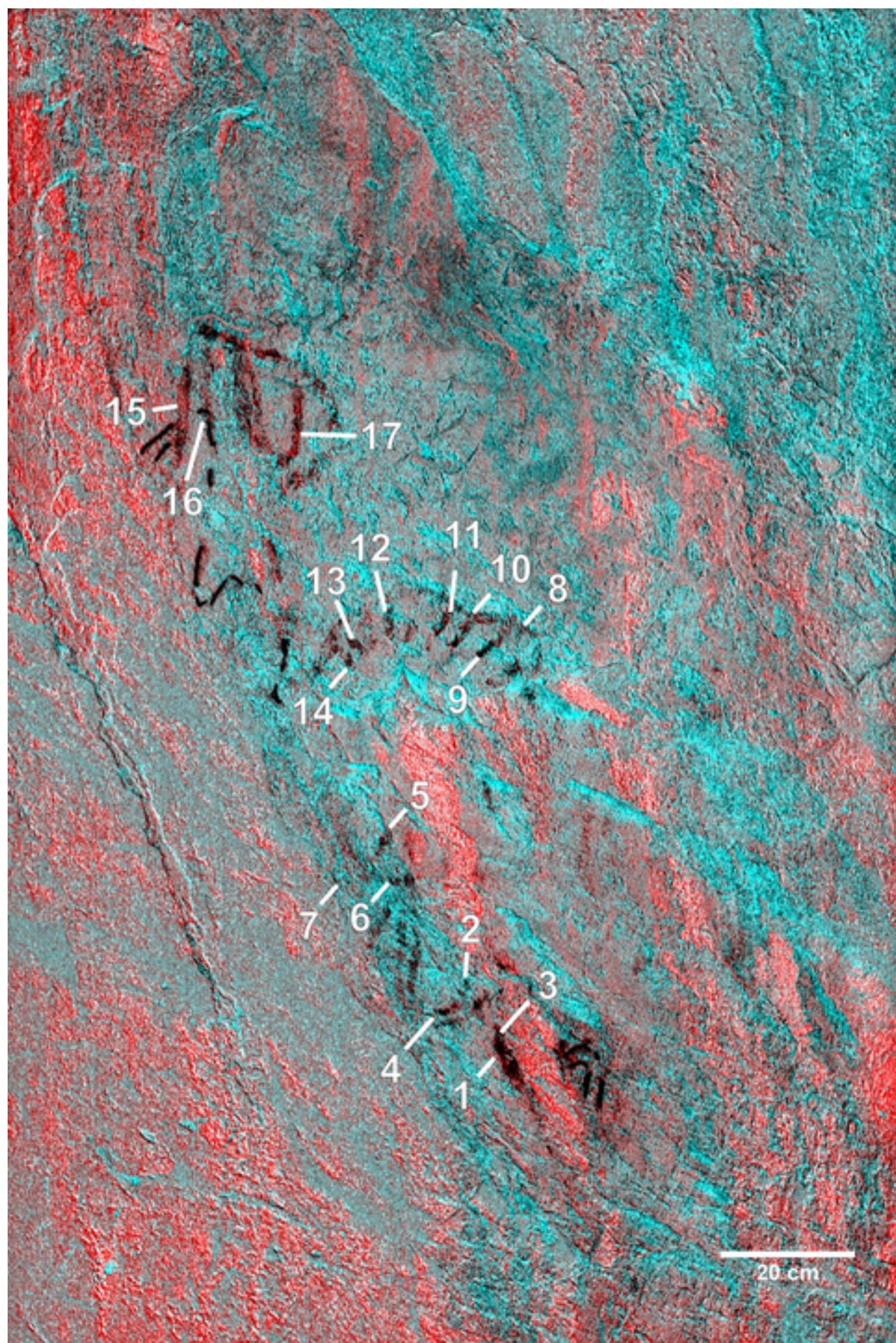


Figure 8
[Click here to download high resolution image](#)

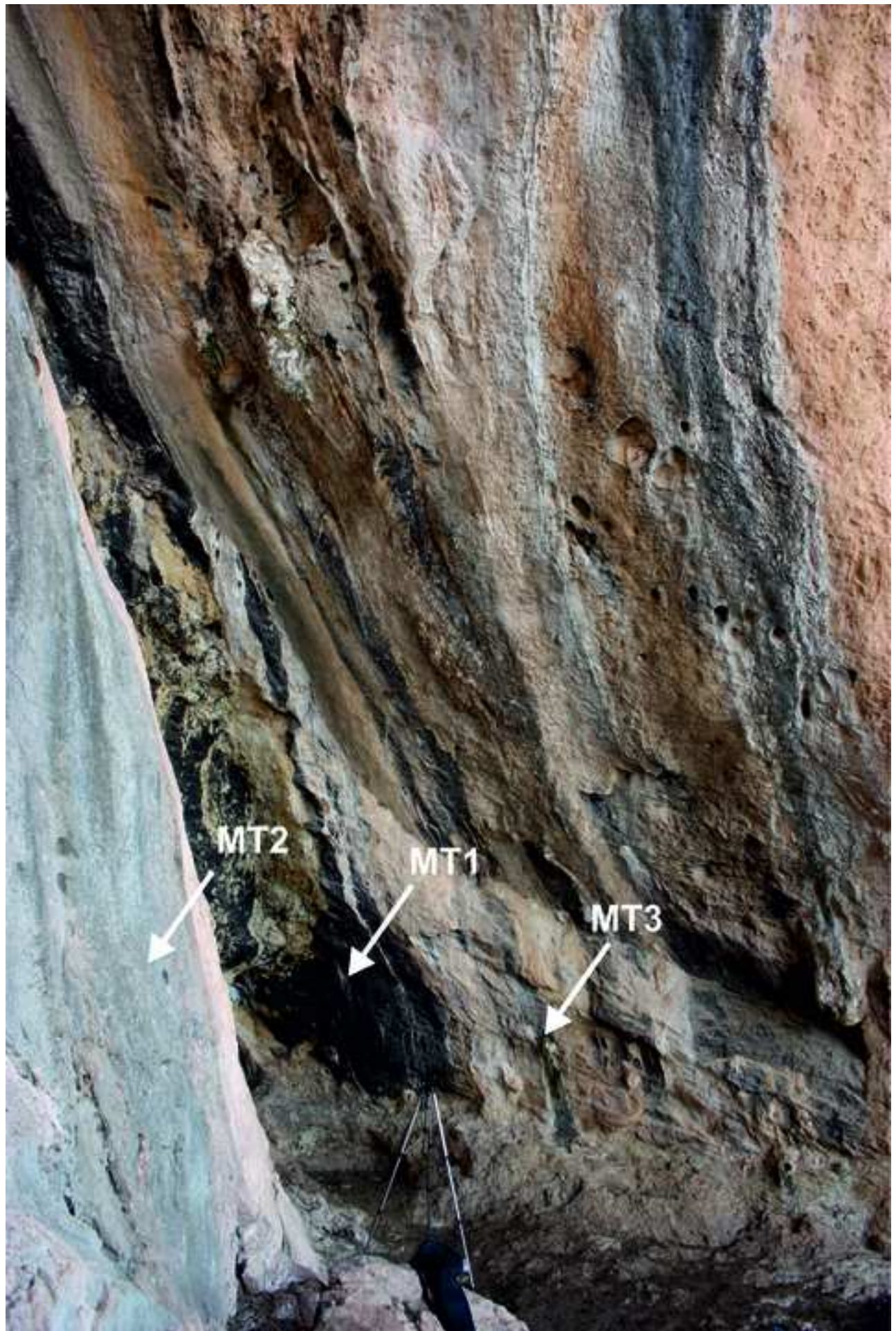


Figure 9
[Click here to download high resolution image](#)

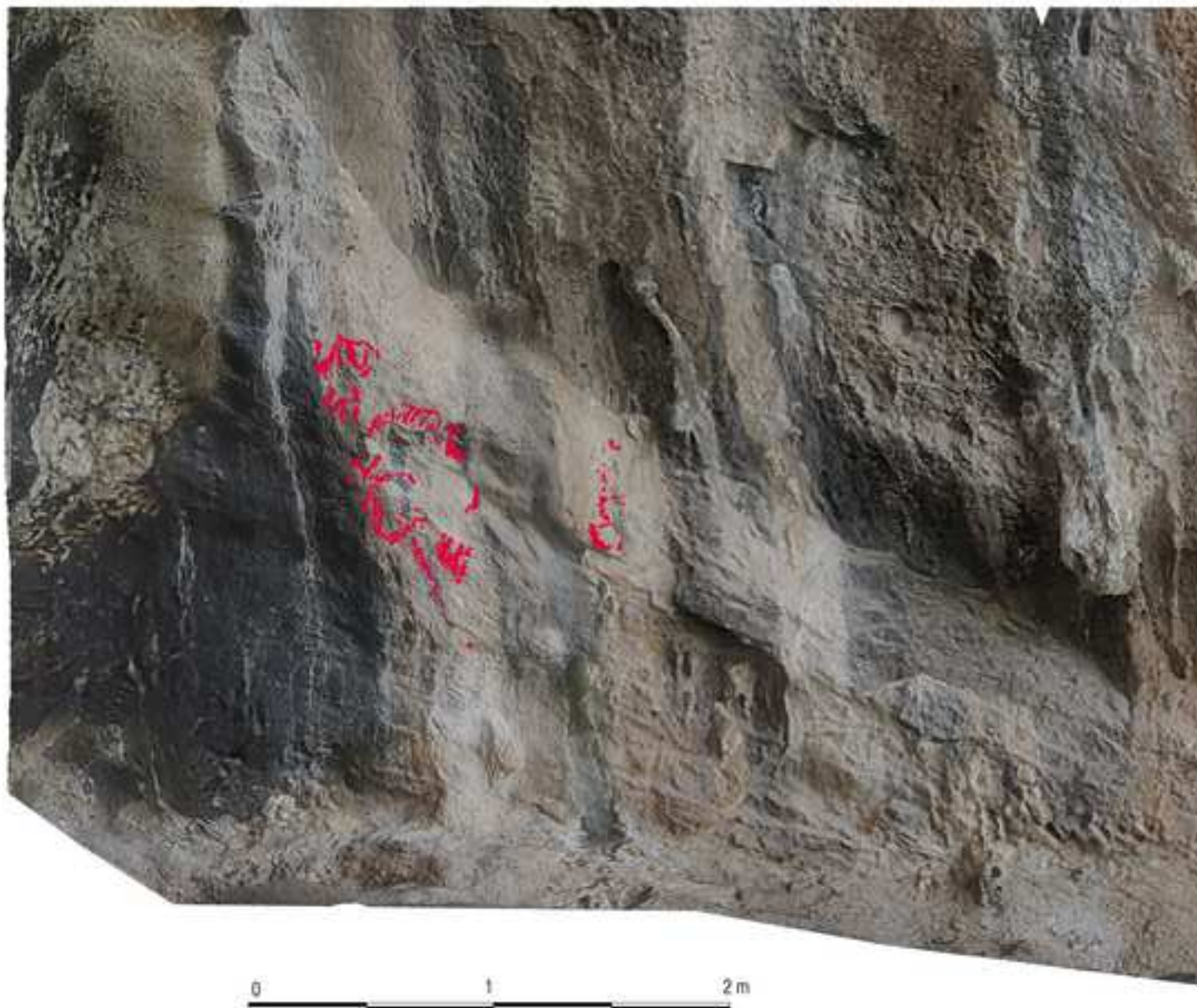


Figure 10
[Click here to download high resolution image](#)

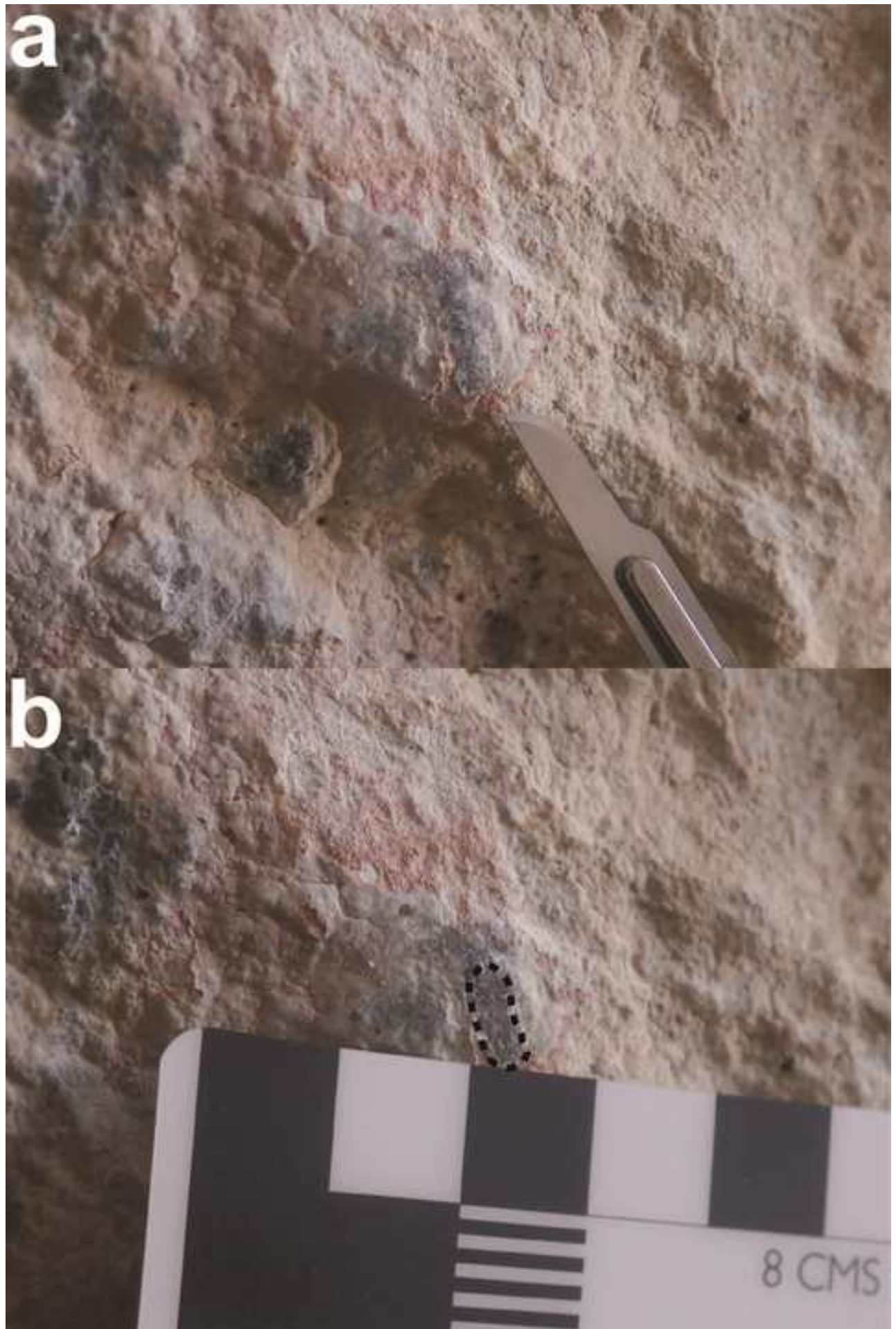


Figure 11
[Click here to download high resolution image](#)

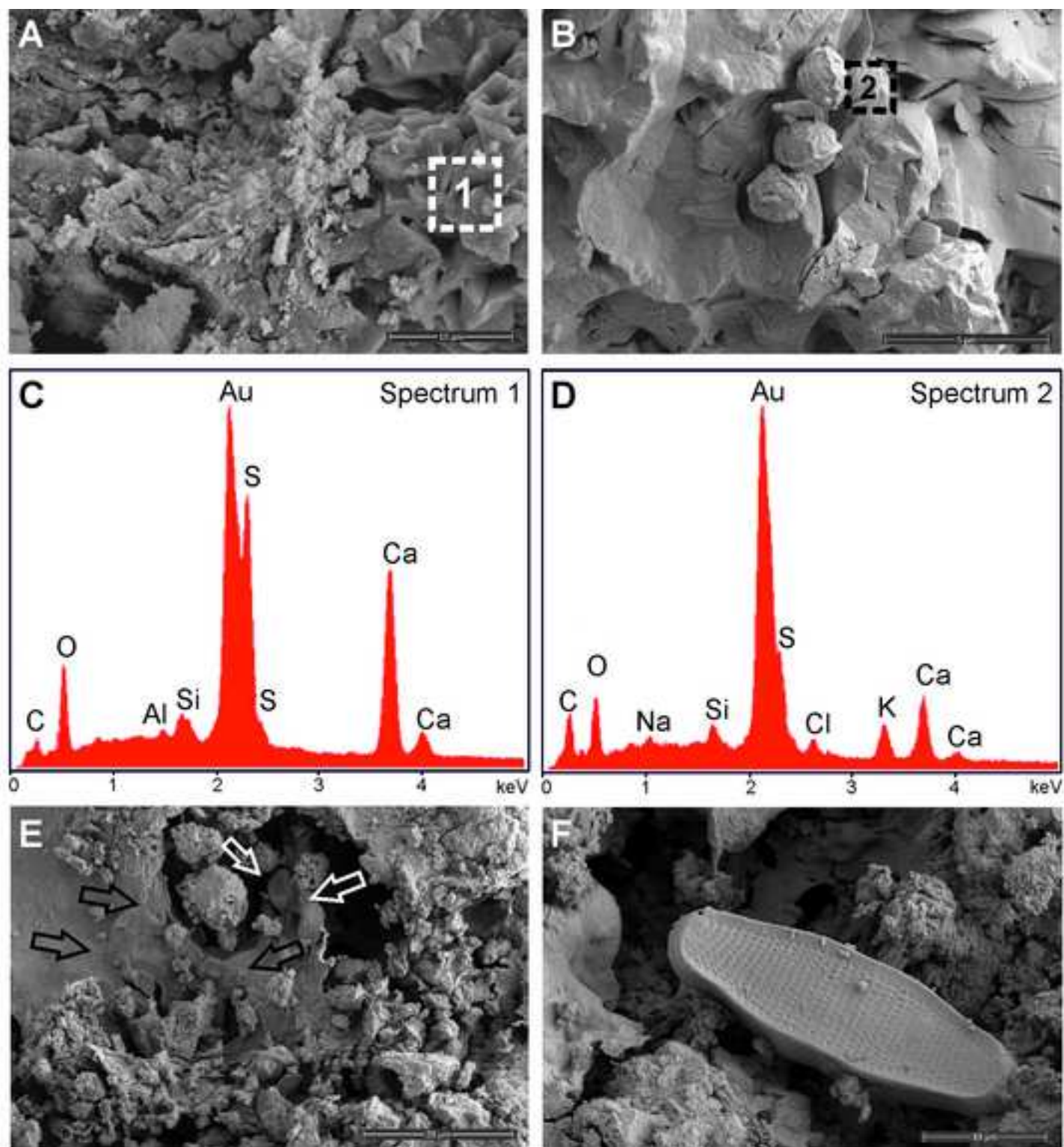


Figure 12

[Click here to download high resolution image](#)

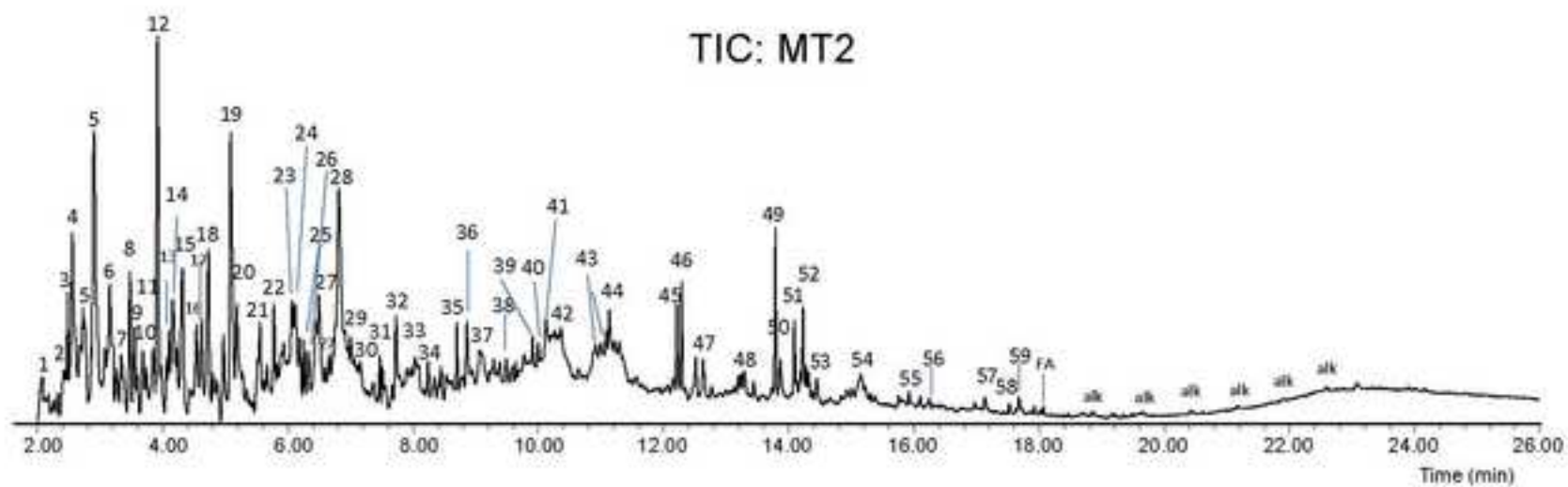


Figure 13
[Click here to download high resolution image](#)

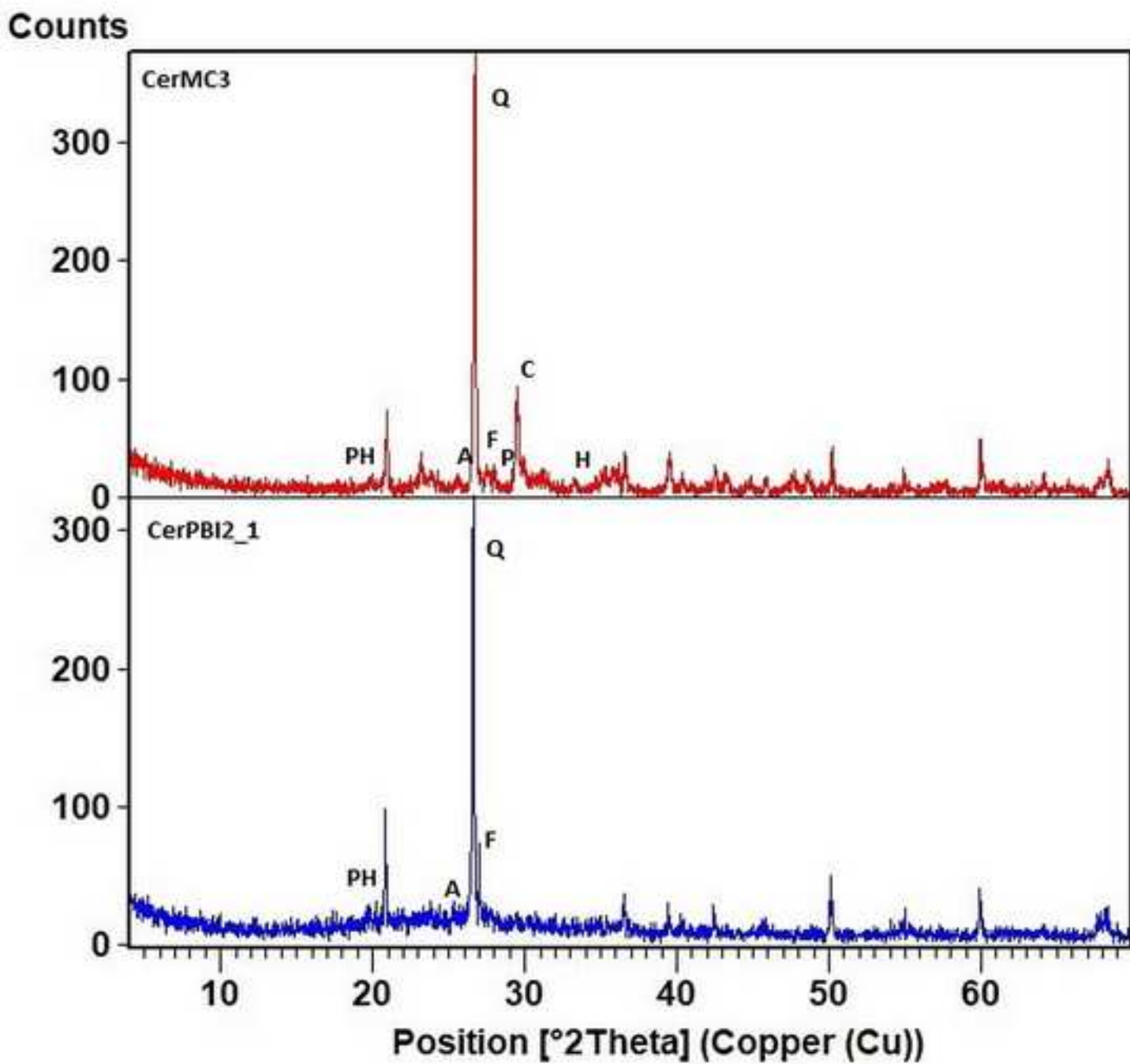


Figure 14

[Click here to download high resolution image](#)

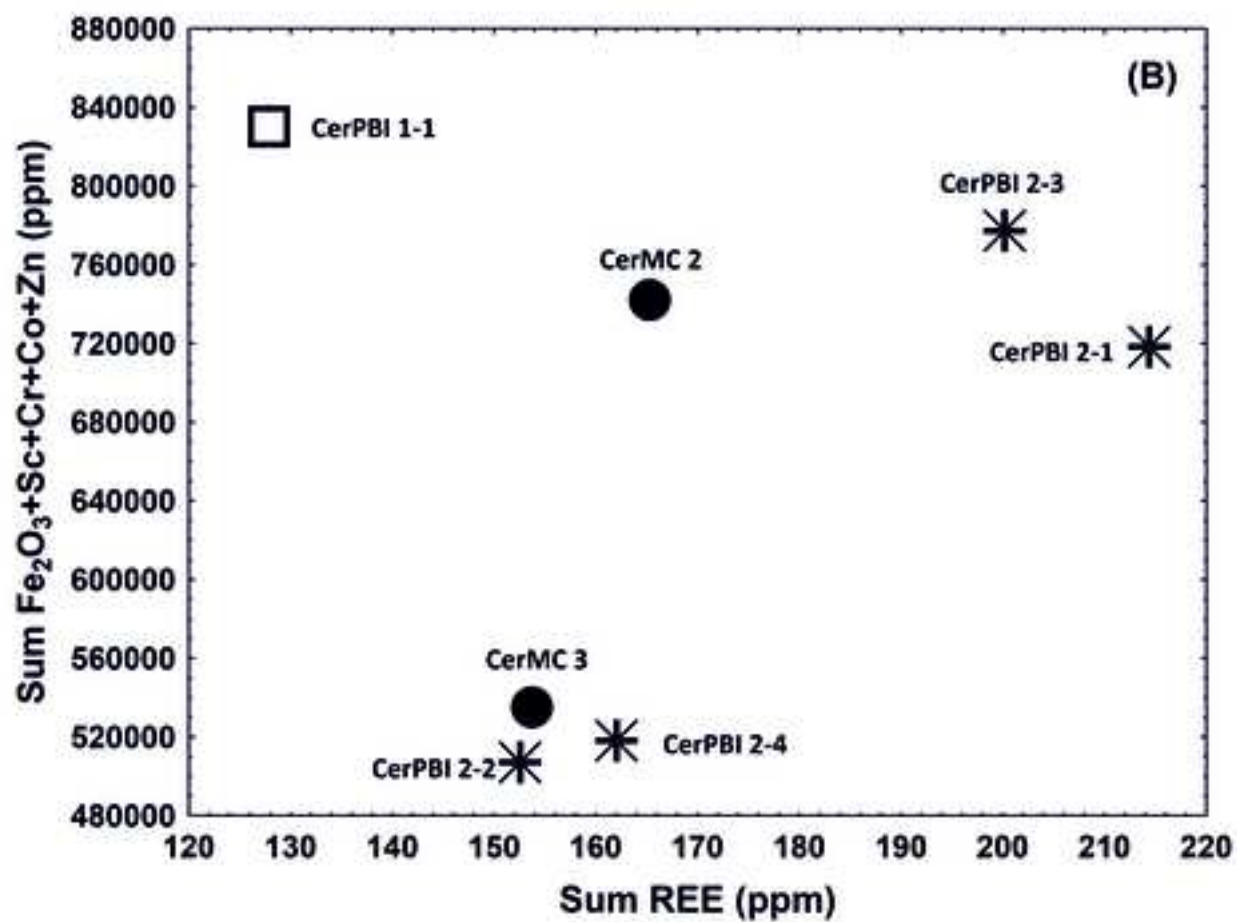
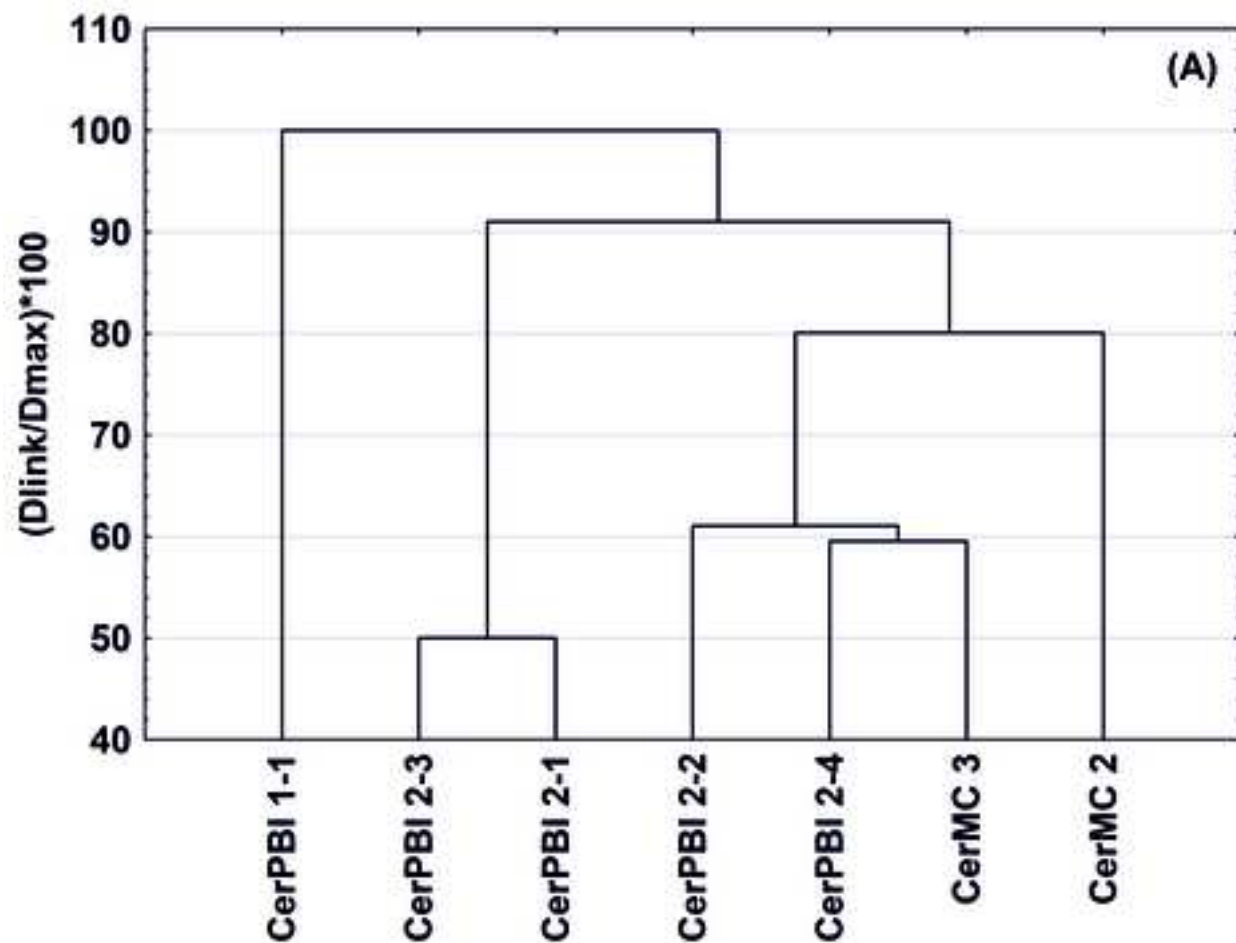


Figure 15
[Click here to download high resolution image](#)

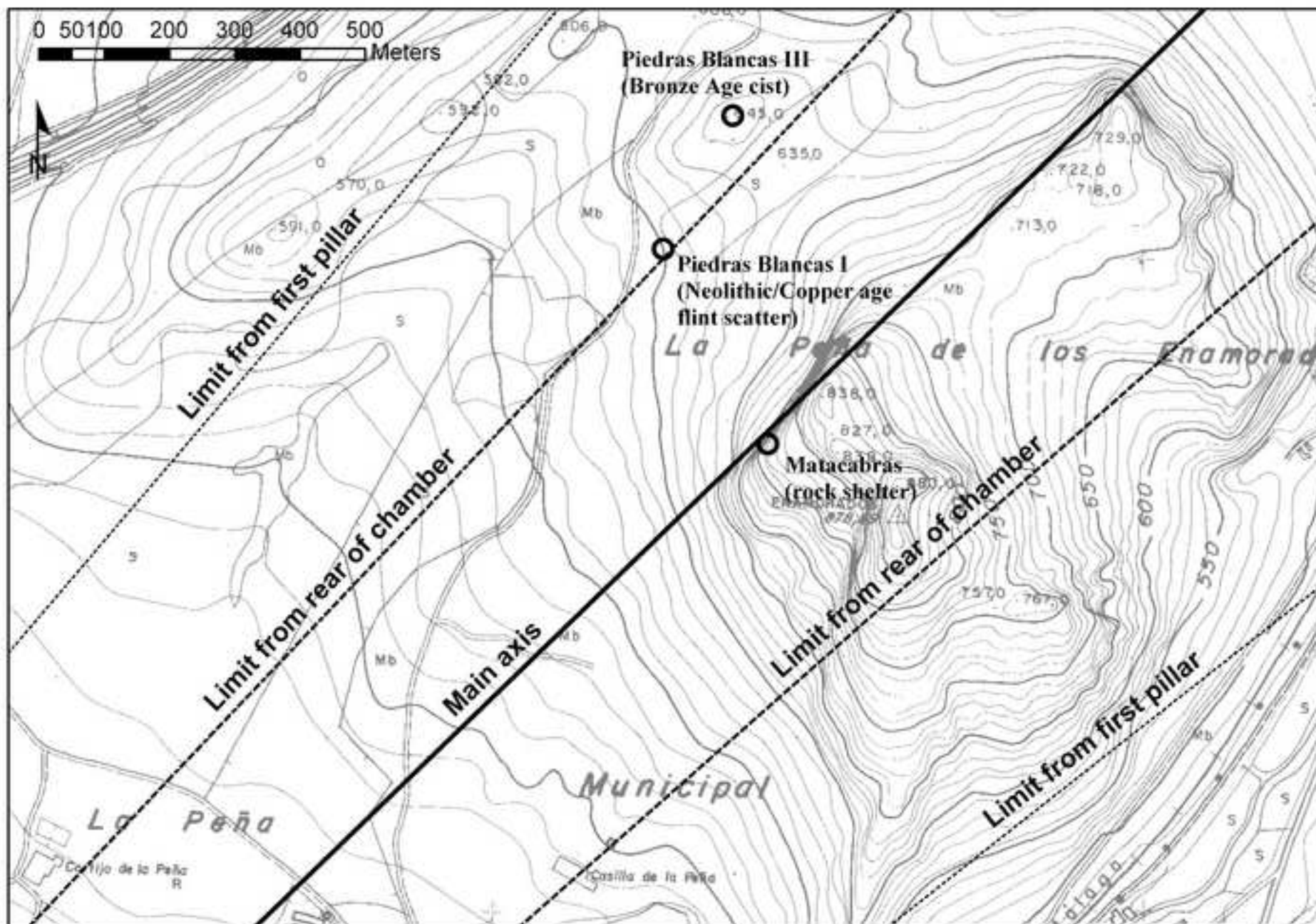


Figure 16

[Click here to download high resolution image](#)

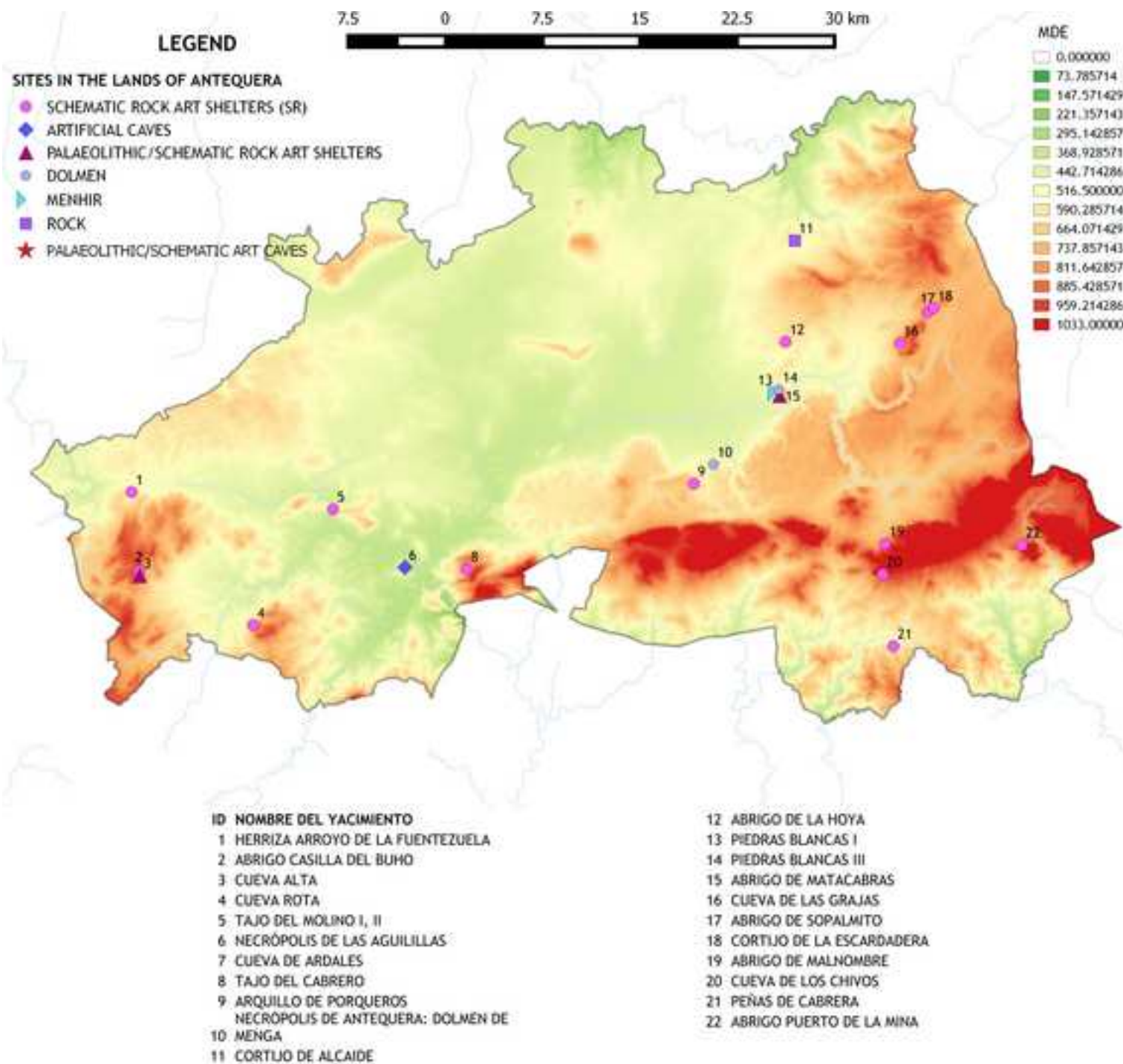


Figure 17
[Click here to download high resolution image](#)

